

THESIS

TRANSPORT-RADIATION FEEDBACKS OF OZONE IN THE TROPICAL
TROPOPAUSE LAYER

Submitted by

Edward Charlesworth

Department of Atmospheric Science

In partial fulfillment of the requirements

For the Degree of Master of Science

Colorado State University

Fort Collins, Colorado

Spring 2017

Master's Committee:

Advisor: Thomas Birner

A.R. Ravishankara
Iuliana Oprea

Copyright by Edward Charleswroth 2017

All Rights Reserved

ABSTRACT

TRANSPORT-RADIATION FEEDBACKS OF OZONE IN THE TROPICAL TROPOPAUSE LAYER

The tropical tropopause layer (TTL) is a region in the atmosphere that shows an interesting combination of tropospheric and stratospheric characteristics over the extent of several kilometers. For example, the TTL shows both convectively-driven tropospheric dynamics and the beginning of the mechanically-driven Brewer-Dobson circulation. The TTL is also important for climate due to its role as the gateway for most air that enters the stratosphere. In this work, a single-column model is used to investigate why a tropical tropopause layer of the observed vertical extent exists. This is done through computations of radiative convective equilibrium temperatures and interactive photochemical equilibrium ozone concentrations. The model uses only a basic simulation of ozone chemistry, convection, and stratospheric upwelling, but the results show that such a simplified expression of critical processes can produce temperature and ozone profiles that are very similar to observations. It is found that vertical transport of ozone by the Brewer-Dobson circulation and its associated effects on radiative heating rates is of first-order importance in producing the observed temperature structure of the tropical tropopause layer, within this simple modeling context. Adiabatic cooling due to stratospheric upwelling is found to be equally important to generate the tropical tropopause layer. With these combined processes, it is suggested that the even the lowest upwelling velocities on the order of observed upwelling can produce a TTL. With regards to climate change through the strengthening Brewer-Dobson circulation, this model suggests that an increase in upwelling from 0.5 to 0.6 mm/s should cool the cold point tropopause by 3.5 K and loft it by half a kilometer.

ACKNOWLEDGEMENTS

This work was funded by the National Science Foundation. Particular thanks go to John Albers for many long and clear descriptions of ozone chemistry and the code that formed the basis of this model. Additional thanks go to Leif Anderson, a stranger who so kindly produced the \LaTeX template for this document and posted it on the internet. The author would also like to thank the faculty of Seattle University, who provided him with a firm foundation in science, and in particular Katie Oliveras and John Carter of the Seattle University Mathematics Department.

TABLE OF CONTENTS

ABSTRACT	ii
ACKNOWLEDGEMENTS	iii
Chapter 1. INTRODUCTION	1
Chapter 2. METHODS	8
2.1. Basic Model Framework	8
2.2. Ozone Chemistry	18
Chapter 3. RESULTS	33
3.1. Radiative Convective Equilibrium and Photochemical Equilibrium without the Full Effects of Upwelling	33
3.2. The Simulation with Transport and Dynamics	43
3.3. The Sensitivity to Climate Change	48
Chapter 4. DISCUSSION	56
4.1. Conclusions	56
4.2. Future Work	58
BIBLIOGRAPHY	61

CHAPTER 1

INTRODUCTION

The term “tropopause” is often used to refer the cold point tropopause (henceforth simply “the cold point”) or the lapse-rate tropopause. The tropopause as a point and not a layer was previously considered to be a sufficient definition for the end of the troposphere and the beginning of the stratosphere for the whole atmosphere. While this is an acceptable description of this transition at higher latitudes, closer examination of the tropical upper troposphere and lower stratosphere motivates a more subtle transition between these regions.

This more subtle transition is called the Tropical Tropopause Layer (henceforth TTL) and is characterized by a mix of tropospheric and stratospheric properties (Fueglistaler et al. [8]). As the name suggests, the TTL lies within the tropics. Vertically, it begins above the level of main convective outflow at approximately 14 km (150 hPa) and ends at approximately 18.5 km (70 hPa). This encompasses the level of zero radiative heating at 15 km (130 hPa) and the cold point tropopause at about 17 km (90 hPa).

Some of these TTL characteristics are chemical. For example, ozone concentrations are dilute in the troposphere (40 ppbv¹) and at their maximum (10000 ppbv) in the stratosphere while the TTL in the climatological mean shows both a local minimum in ozone concentrations and in the higher parts a rapid increase in ozone concentrations. Similarly, water vapor is most densely concentrated and decreasing with height in the troposphere while it is very dilute in the stratosphere.

¹The unit “ppv” refers to parts per by volume. Additional characters such as “m” and “b” refer to “million” and “billion”, so that “ppbv” reads “parts per billion by volume”.

The TTL also contains a mix of tropospheric and stratospheric dynamics. Precisely, while convection dominates the dynamics of the tropical troposphere there is nearly no convection that reaches beyond the cold point. Dynamics in the stratosphere, instead, are dominated by the mechanically-driven Brewer-Dobson circulation. The TTL serves as the transition between these two regimes, where convection penetrates the lower layers (and occasionally higher) and the Brewer-Dobson circulation gradually takes over.

We might ask why these characteristics are not simply divided between the troposphere and stratosphere. Why should the tropical tropopause not be a sharper border as we see at other latitudes? Why, instead, do these stratosphere-troposphere transitions occur over a region that is nearly a third as tall as the troposphere itself? This work is set upon answering the question of why the TTL exists.

Understanding of the TTL is also important due to its role as the gateway to the stratosphere for most of the air that enters it. This occurs through the action of the aforementioned Brewer-Dobson circulation. This feature, depicted in Figure 1.1, carries air from the tropics into middle and higher latitudes. The Brewer-Dobson circulation is expected to strengthen due to climate change.

Most water vapor in the stratosphere has entered through the TTL. The amount of water that enters is largely set by the temperature of the cold point, making TTL temperatures critical for the radiative impacts of water in the stratosphere (Fueglistaler et al. [8]). Similarly, chlorofluorocarbons that cause ozone depletion enter the stratosphere largely through the TTL. Therefore, another important question about the TTL is how its structure may change under climate change. Because heating rates in the TTL are very small, seemingly

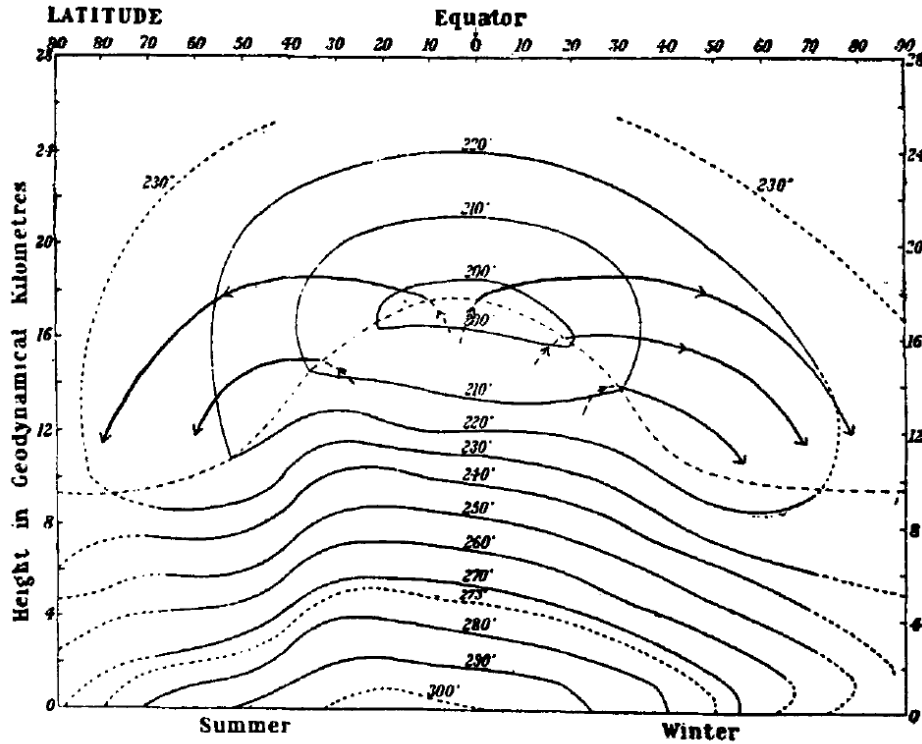


FIG. 5. Isotherms over the Globe
 A supply of dry air is maintained by a slow mean circulation from the equatorial tropopause.

FIGURE 1.1. A conceptual depiction of the stratospheric circulation from Brewer [5].

minor differences in calculated heating rates can produce large changes in TTL temperatures. This makes the investigation of the TTL climate sensitivity very difficult in climate models, so much that climate models present approximately a 10 K range in tropopause temperatures (Gettelman et al. [9]). This is illustrated in Figure 1.2.

Both early and recent work on the TTL has established that the temperature structure of the TTL is sensitive to water vapor concentrations (Manabe and Strickler [12], Birner and Charlesworth [3]). At least one study (Thuburn and Craig [17]) has suggested that the TTL is sensitive to carbon dioxide and that in fact the TTL exists due to carbon dioxide heating in between the cold point and convection top. Other work suggests upwelling can reduce the

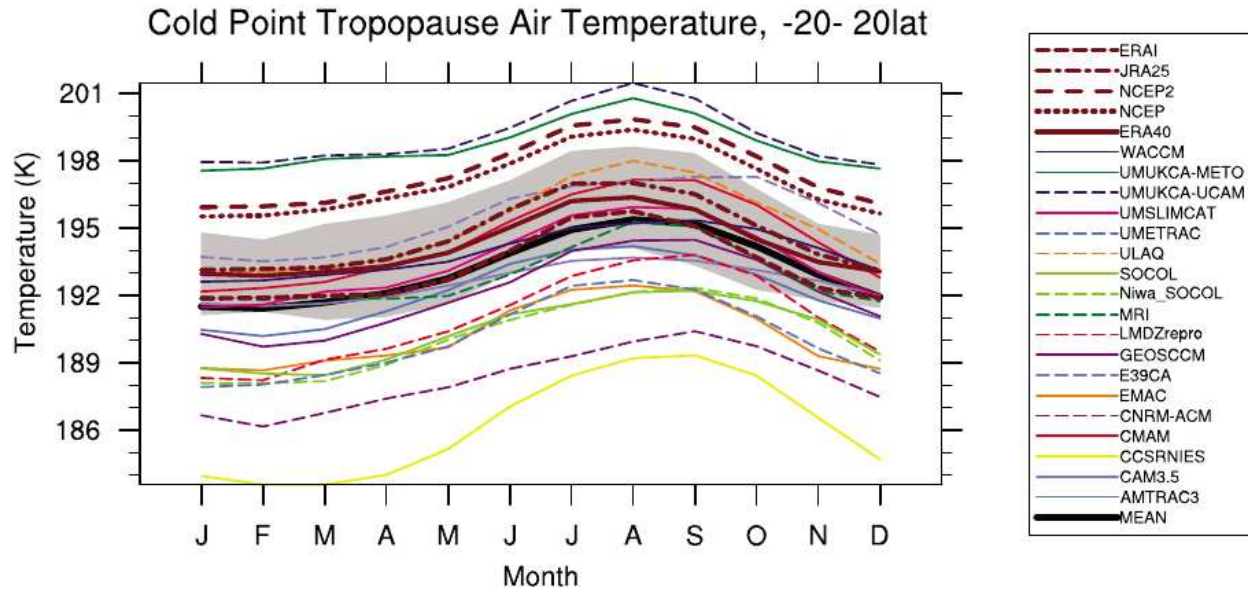


FIGURE 1.2. The range of cold point temperatures from a large number of climate models from Gettelman et al. [9].

impact of water vapor on TTL temperatures through lofting of the cold point by dynamics heating (Birner and Charlesworth [3]).

Some work has also expressly investigated the effect of stratospheric dynamics on TTL temperatures (Thuburn and Craig [17], Birner [2]). One study has suggested transport-radiation feedbacks involving stratospheric water vapor and upwelling (Birner and Charlesworth [3]). Other studies have noted that stratospheric upwelling must provide an impact on TTL temperatures through the transport of ozone and consequent ozone concentration modulations, as well as the transport of ozone through horizontal advection (Thuburn and Craig [17], Konopka et al. [11]).

Some earlier work has suggested that the TTL is sensitive to ozone concentrations as well (Thuburn and Craig [17], Birner and Charlesworth [3], McElroy et al. [13]). Other work has suggested the height at which ozone rapidly increases can provide an upper limit for the cold point altitude (Thuburn and Craig [17], Birner and Charlesworth [3]). Some radiative convective equilibrium work has also investigated the impact of artificial changes in ozone on

equilibrium temperatures in the TTL (Thuburn and Craig [17], McElroy et al. [13], Birner and Charlesworth [3]). Other work has also noted that the stratospheric circulation can have a significant impact on TTL temperatures through both dynamics and transport of ozone (Fueglistaler et al. [8]).

More recent work has suggested that differences in ozone alone could explain a majority of the inter-model cold point temperature variability (Birner and Charlesworth [3], Gettelman et al. [9]). Ozone concentrations are also expected to be significantly altered as climate change progresses, as shown in Figure 1.3. Some amount of this trend is expected to be caused by the strengthening of the Brewer-Dobson circulation, particularly in the lower stratosphere. This is because ozone concentrations in this region are strongly controlled by transport processes, as depicted in Figure 1.4.

However, to the knowledge of the author, no published work has investigated the simultaneous impact of dynamics and transport of ozone on the temperature structure of the TTL in a mechanistic framework, despite the noted importance. This is the goal of this work, and should be seen as an extension of the work of Thuburn and Craig [17] and Birner and Charlesworth [3]. In this pursuit, simultaneous calculations of clear-sky radiative convective equilibrium and photochemical-transport equilibrium have been performed. A standard radiative transfer method (RRTMG) for computations of radiative heating rates has been used, alongside the convective adjustment method of Thuburn and Craig [17] for a convective parameterization and simplified stratospheric dynamics to simulate the temperature change due to stratospheric upwelling.

Beyond this introductory chapter, the second chapter of this work discusses the model framework and is separated into two sections. The first section includes the radiative transfer

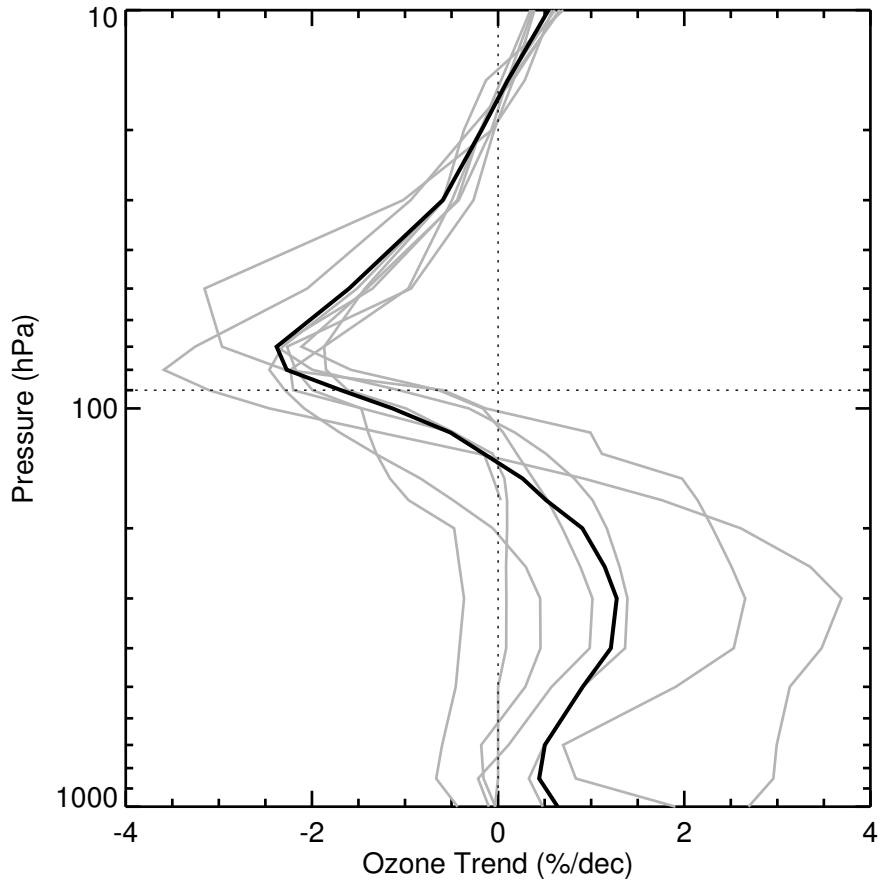


FIGURE 1.3. Decadal tendency of ozone for some climate models. Based on top left panel of Fig. 18 in Gettelman et al. [9], courtesy Thomas Birner.

methods used, the vertical structure of the model, the application of dynamics, and the treatments of fixed chemical species and water vapor. The first section also documents the control experiment of the model and the application of dynamics on this. The second section of the second chapter describes stratospheric ozone chemistry as applied in this model. The third chapter of this work discusses the results of interactive ozone chemistry in radiative convective equilibrium and is separated into three sections. The first section provides a short discussion of the temperature and ozone sensitivities to the separate processes of dynamics and transport and is followed by a description of the impact of simultaneous dynamics and transport. This second section represents the key result of this work as it shows that transport

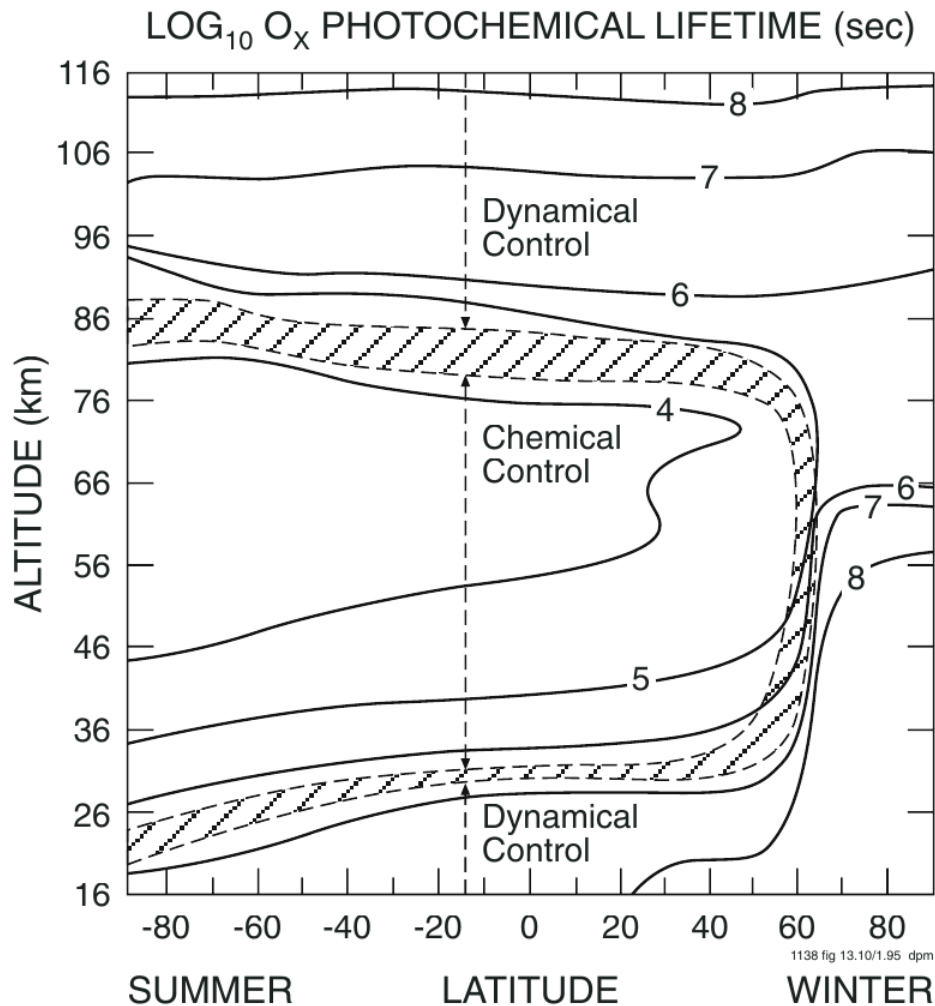


FIGURE 1.4. A depiction of the chemistry dominated (“Chemical Control”) and transport-production dominated (“Dynamical Control”) regimes of ozone from Brausseau and Solomon [4]. Contours show the lifetime of odd-oxygen by chemistry. In stratosphere this lifetime is to a good approximation the chemical lifetime of ozone.

is a necessary process and suggests dynamics as the additional reason for the existence of the TTL. The third section discusses the sensitivity of the TTL to changes in upwelling that may occur due to climate change, as well as the sensitivity of the TTL to a broader range of upwelling velocities.

CHAPTER 2

METHODS

2.1. BASIC MODEL FRAMEWORK

The basic method used in this work is the calculation of equilibrium profiles of temperature and in a single column. The method for the calculation of equilibrium ozone profiles is described in section 2.2. In the present section, the method used for the calculation of equilibrium temperature profiles is described.

The term *radiative convective equilibrium*, previously mentioned in the introductory chapter, refers to the calculation of equilibrium profiles of temperature. This method involves the calculation of temperature profiles through the transfer of short-wavelength, high-energy solar radiation and long-wavelength, low-energy longwave radiation. Pure radiative equilibrium temperature profiles show very rapid decreases in temperature near the surface. In the real atmosphere, these sharp gradients are not observed because they provide an impetus for the process of convection which transfers energy from the lower layers of the atmosphere to the higher layers. For a realistic simulation of equilibrium temperatures in the atmosphere, then, both radiation and convection are required, and therefore the equilibrium obtained is called radiative convective equilibrium (henceforth RCE). RCE has been used in several forms in many preceding works, most notably the pioneering work of Syukuro Manabe [12].

The model used in this work implements a single-column structure, where the atmosphere simulated is a vertical section of the atmosphere with no defined horizontal dimensions, aside from the fixed latitude of the model atmosphere. For the present work the latitude selected

is 10 S, to maintain consistency with the SHADOZ dataset which is used as a reference in this work.

Because this work seeks to predict the vertical extent of the TTL using simplified measures, we define the TTL for this work as beginning at the convection top and ending at the cold point tropopause. This definition is consistent with defining the TTL in the observed atmosphere as existing between the clear-sky level of zero radiative heating at 15.5 km (125 hPa) and the observed cold point tropopause at 17.3 km (90 hPa). While the latter boundary is clear, the former may not be. The level of clear-sky zero radiative heating is the altitude at which clear-sky sinking gives way to clear-sky upwelling, and in the real atmosphere this is higher than the convection top. However, in the present model convection behaves in a simplified manner so that the level of clear-sky zero radiative heating and the top of convection are at the same altitude. This definition is also consistent with previous investigations of RCE in the TTL (Thuburn and Craig [17], Birner and Charlesworth [3]).

The model column uses 194 layers, (to the author’s knowledge this is more than any other RCE work aside from Birner and Charlesworth [3]) each at a fixed altitude. Each layer has associated variables of pressure, temperature, and chemical mixing ratios. Radiative trace gases exist for H₂O, CO₂, O₃, N₂O, CO, CH₄, O₂. Of these, only H₂O and O₃ are interactive in this model. The calculation of water mixing ratios is described in the following paragraphs of this section while the calculation of ozone mixing ratios is described in section 2.2. The other chemicals have prescribed vertically-uniform mixing ratios that are the same in every experiment described in this work. These mixing ratios are $\chi_{\text{CO}_2} = 356$ ppmv, $\chi_{\text{N}_2\text{O}} = 320$ ppbv, $\chi_{\text{CO}} = 100$ ppbv, $\chi_{\text{CH}_4} = 1.75$ ppmv, $\chi_{\text{O}_2} = 0.21$ ppv, chosen to maintain consistency with Thuburn and Craig [17]. Every layer is also associated with two levels, one above and

one below, and each level is associated with two layers, one above and one below, aside from the surface level and the top-of-model level which are only associated with the lowest layer and highest layer, respectively. Each level has a fixed altitude and associated variables of temperature and pressure, and serve as boundaries for layers.

The altitude scheme used begins at the surface level at 0 km and increases this altitude by 200 meters for each following level until an altitude of 32 km is reached. After this a constant pressure spacing of 0.3 hPa is used to determine the initial level pressures. The level pressures are then used to calculate fixed altitudes for each level, based on an assumed exponential with height expression for pressure. The scale height used for this expression is 7 km.

The pressures of layers are taken to be the average of the pressures of the bounding levels for each layer. The layer pressures are computed on each time step by integrating the hydrostatic equation from the surface level pressure, which is 1013 hPa. On every time step the level pressures are recomputed so that the relationship of each layer pressure to its corresponding levels is maintained. Precisely,

$$p_{n+1} = 2p_{n+\frac{1}{2}} - p_n,$$

where n denotes a level p denotes a pressure, and $n + \frac{1}{2}$ denotes a layer. This layer-as-average-of-levels relationship is also assumed for the layer and level temperatures, and the relationship is maintained on every time step after the application of temperature changes with a boundary condition of 300 K for the surface level. These layer temperature changes are produced through three processes. Two of these processes are used in every experiment

- radiative transfer and convective adjustment - while the third processes - adiabatic cooling due to stratospheric upwelling - is used in some but not all experiments.

Radiative heating rates are computed through the use of the Rapid Radiative Transfer Model (RRTMG), a radiative transfer model produced by the Radiative Transfer Working Group of Atmospheric and Environmental Research (Mlawer et al. [15]). This radiative transfer model uses the correlated-k method to efficiently compute solar and terrestrial radiation fluxes and atmospheric heating rates. RRTM is used on every time step to compute radiative heating rates for each model layer.

Convective adjustment is simulated using the method applied in Thuburn and Craig [17]. Precisely, a vertically-uniform critical convective temperature lapse rate¹ is chosen. When convective adjustment is applied the lapse rate at each layer is set to the critical convective temperature lapse rate if it exceeds the value, so that temperatures that are too low are increased. For this work, the critical convective temperature lapse rate is fixed to -6.5 K/km for all experiments. This value is chosen because it is commonly used (e.g. Manabe and Strickler [12]) and because it is consistent with the choice of Thuburn and Craig [17] and Birner and Charlesworth [3].

The third and final process that causes model temperature changes is dynamics, simulated through stratospheric upwelling. This upwelling causes temperature changes through temperature advection and adiabatic cooling. The dynamic heating rate applied by this is given by

$$\frac{\partial T}{\partial t} = \bar{w}^* \left(\frac{\partial T}{\partial z} + g/C_p \right),$$

¹A lapse rate is the rate of decrease in a quantity with increasing altitude.

where T is temperature, z is altitude, \bar{w}^* is the upwelling velocity, g is gravity, and C_p is the heat capacity of air at constant pressure. This process only occurs above the convection top in this model because temperature changes due to upwelling that occurs in the troposphere are balanced by clear-sky sinking and radiative cooling.

In addition to temperature and pressure changes, the model used in this work also applies changes to water vapor concentration. This process computes water vapor concentrations separately for three regions - the troposphere, the TTL, and the stratosphere. Water vapor concentrations in the troposphere are computed based on a fixed 50% relative humidity and the calculated saturation vapor pressure for each layer. To compute water vapor mixing ratios in the TTL, the fractional decrease in water vapor between the convection top layer and the layer below it is applied as the fractional decrease in water vapor mixing ratio for all the layers above the convection top layer until a prescribed stratospheric water vapor concentration is obtained. Precisely, for a convection top at layer number n_{CT} , the fractional decrease of water vapor mixing ratio χ is $\gamma = \frac{\chi_{n_{CT}}}{\chi_{n_{CT}-1}}$. This is applied to every subsequent level so that the water mixing ratio at layer $n_{CT} + x$ is $\chi_{n_{CT}}\gamma^x$. For the present work, all experiments use a prescribed stratospheric water vapor mixing ratio of 4 ppmv. This is consistent with the control case of Birner and Charlesworth [3] where it was chosen based on observations. After the prescribed stratospheric water vapor mixing ratio is obtained, all higher layer water mixing ratios are fixed to this value. This process is necessary to transition the water vapor profile from the tropospheric and stratospheric profiles because there is no guarantee that relative humidity and saturation vapor pressure alone will reduce calculated water vapor concentrations to the prescribed value for the stratosphere.

This behavior can be seen in Figure 2.1, which shows profiles from the result of two 500 day RCE experiments. The integration time of 500 days was chosen because of the long radiative time scales near the cold point, which are on the order of 50 days. The first experiment used model control parameters and data, so that dynamics did not affect the temperatures profiles of the experiment. The second experiment used the same parameters except that dynamics through a 0.5 mm/s stratospheric upwelling was applied. For this figure, and for all other figures in this document, the plotted quantities are averages of the last 20 days of computation.

In fact, the temperatures in the case with dynamics are nearly 21 K less than the case without dynamics, around 19 km. The cold point lofts and cools from approximately 207 K and 15 km in the case without dynamics to 191 K and 18 km in the case with dynamics. The convection top has raised and cooled similarly. This shift brings the cold point temperature to the observed value of 191 K. In altitude, the calculated cold point is just a kilometer higher than the observed 17 km cold point. This change is due to the introduction of dynamics, which produces a cooling of a little more than 0.4 K/day at the dynamically-affected cold point.

This dynamic heating rate can be compared to the radiative heating rates in Figure 2.2. From the full-column figure it is clear that the dynamic heating rates are small compared to the radiative heating rates above about 25 km. Below about 15 km, the dynamic heating rates are zero because this is the level of the convection top and upwelling is not applied below it. Because the radiative heating rates are much larger than the dynamic heating rates in the higher atmosphere, the temperature changes due to dynamics in this region are small.

Between 15 and 25 km, however, the dynamic heating rates are very significant. In fact, the dynamic heating rates are such a significant forcing on the profile that the longwave heating rates become positive between about 16 and 21 km and are most positive just above the cold point. In fact, between 17.5 km and 19 km the longwave heating rates are stronger than the shortwave heating rates. This is a fundamental change from the longwave heating rates of the control case, where all longwave heating represents a cooling for the atmosphere. The dynamic heating, however, is strong enough to cool profile temperatures so much that they emit less longwave radiation than they absorb.

The greatest changes in temperature occur near the cold point. This is unsurprising, since the location where the most cooling occurs should logically become or reside near the final cold point. However, the fact that the dynamically-affected cold point exists where radiative heating rates are smallest is perhaps surprising. This makes sense, however, when it is considered that longwave emission depends approximately on the fourth power of temperature while shortwave heating generally does not depend strongly on temperature. Precisely,

$$cT^4 = L + S + D,$$

where T is the temperature at equilibrium, S is the shortwave heating rate, D is the dynamic heating rate, c is a constant, L is the longwave heating absorbed, and cT^4 is the longwave heating emitted. The temperature that balances a given dynamic heating rate and shortwave heating rate is then

$$T = \left(\frac{L + S + D}{c} \right)^{1/4}.$$

Based on this description, it is clear that for a given dynamic heating rate the largest change in equilibrium temperature should occur where the shortwave heating rate and longwave

absorption are smallest, since the equilibrium temperature depends approximately on the fourth root of the sum of shortwave radiative, longwave absorption, and dynamic heating.

The fact that the cold point occurs where shortwave heating rates are lowest is therefore logical, since this is where dynamic heating can have the largest impact. Conversely, higher layers show greater shortwave heating rates and are therefore less changed by dynamic heating of the magnitudes shown. If the shortwave heating rates at the level of the cold point were much larger, however, the dynamic heating rates shown would have substantially less impact on equilibrium temperatures.

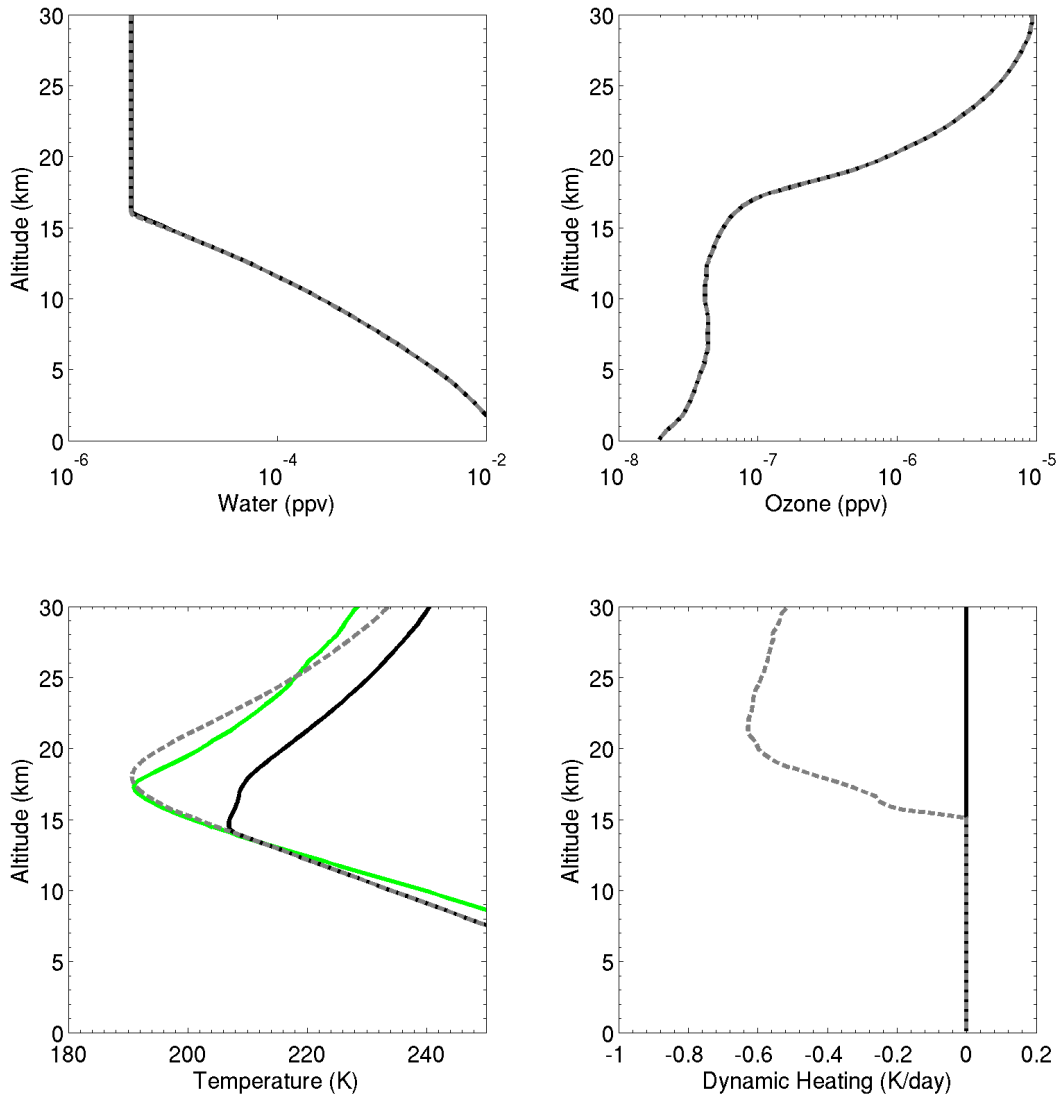


FIGURE 2.1. Profiles of variables resulting from a 500 day RCE computation using control parameters and data (black solid line) and a similar computation except for the addition of dynamics through 0.5 mm/s stratospheric upwelling (gray dashed line). Top left: water mixing ratio. Top right: ozone mixing ratio (from SHADOZ dataset). Lower left: temperature. Lower right: dynamic heating rates. Green solid line shows observed temperature profile from the SHADOZ dataset.

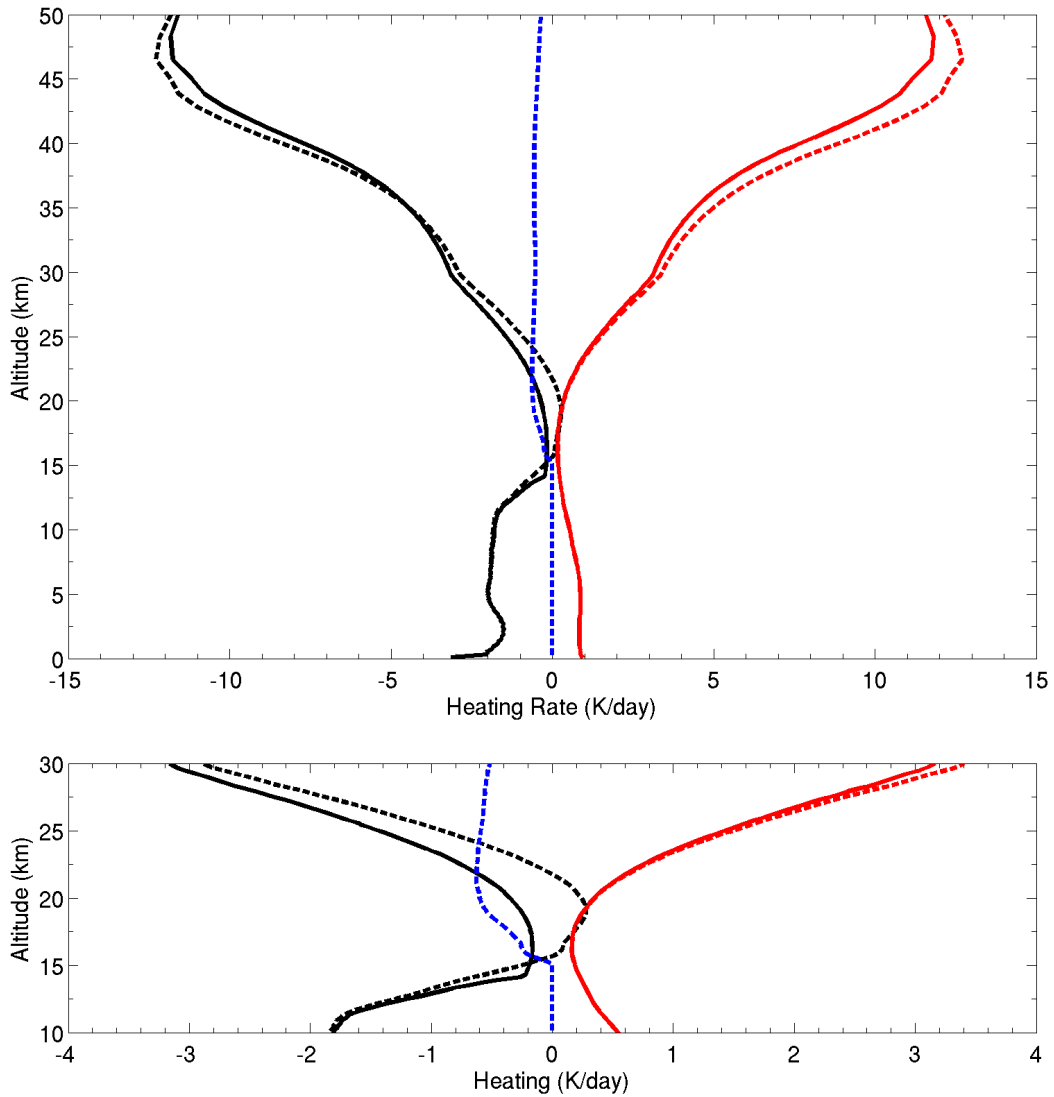


FIGURE 2.2. Profiles of heating rates from shortwave radiation (red) and long-wave radiation (black) resulting from a 500 day RCE computation using control parameters and data (solid lines) and a similar computation except for the addition of dynamics through 0.5 mm/s stratospheric upwelling (dashed lines). Top: full column profiles. Bottom: same as top, but focused on TTL region. The blue dashed lines shows the dynamic heating rate from the experiment with applied upwelling.

2.2. OZONE CHEMISTRY

A complete simulation of ozone chemistry involves tracking dozens of chemicals and detailed chemical reaction information for each, creating an environment with a great deal of complications and factors to be considered. However, the basic description of stratospheric ozone chemistry is relatively straightforward to describe and implement. Because the purpose of this work is to understand the qualitative relationship between ozone, chemistry, radiation, and transport in the TTL, a simplified model is preferable as long as it captures the fundamental behavior of ozone chemistry. Conversely, more precision could be obtained with a complete model but the complications of so many additional variables and processes would make understanding more difficult to obtain. Simplified modeling in this way is the preferable method to create a platform for understanding the fundamental processes involved in ozone chemistry and its relationships to other processes in the TTL, and is therefore utilized in this work.

The fundamental processes of stratospheric ozone chemistry are referred to as *pure oxygen chemistry*. This is often called Chapman chemistry, after Sydney Chapman who first described the formulation in 1930. The model describes the chemistry of ozone in stratosphere with respect to oxygen species alone. This chemistry model, however, produces far lower chemical loss rates than are observed. Computation of reasonable chemical loss rates requires the addition of catalytic cycles of ozone destruction through the chemistry of nitrogen, chlorine, and hydrogen species.

In more chemically focused work, an additional accounting of aerosol chemistry is required to compute appropriate contributions from each catalytic cycle species. Without accounting for aerosols, the relative contributions of each catalytic species are skewed, although the

total quantity of ozone destruction is approximately the same (Jacobs [10]). However, this work only requires that the chemical production and loss of ozone are at reasonable values to describe the real atmosphere, and therefore aerosol simulations are not required.

For this reason, the only necessary chemistry is the chemical production of ozone, which only occurs through pure oxygen chemistry, and the chemical destruction of ozone through pure oxygen chemistry as well as the catalytic cycles of ozone destruction in the absence of aerosols. In this absence, nitrogen species happen to provide the greatest contribution of ozone destruction for most altitudes in the atmosphere. Therefore the only chemistry simulated in this work is that of the odd-oxygen species which are ozone (O_3), diatomic oxygen (O_2), and monatomic oxygen (O or O^*)², as well as the chemical destruction of ozone by NO_2 .

Two additional processes can change ozone concentrations in this simulation. The first is transport through stratospheric upwelling, while the second is the boundary value of ozone mixing ratios based on a tropospheric value. This latter process simulates the rapid transport of tropospheric ozone, which is approximately uniform for the free troposphere, through convection so that ozone does not exceed a minimum value.

The complete ozone continuity equation used in this work is

$$(1) \quad \frac{d\chi_{O_3}}{dt}(z) = P - L_{O_x}\chi_{O_3}^2 - L_{NO_x}\chi_{O_3} - \bar{w}^* \frac{\partial \chi_{O_3}}{\partial z},$$

where

$$P = 2J_{O_2}\chi_{O_2},$$

²In chemistry-focused work, ground-state monatomic oxygen will sometimes be indicated by $O(^3P)$ while excited-state monatomic oxygen will be indicated by $O(^1D)$, where these additional symbols of 3P and 1D indicate the state of the highest-energy orbital occupied by an electron. However, this project investigates topics beyond ozone chemistry, so for the simplicity of notation the symbol O will refer to ground-state monatomic oxygen while O^* will refer to excited-state monatomic oxygen.

is the chemical production of ozone,

$$L_{O_x} = \frac{2J_{O_3}k_3}{k_2\chi_{O_2}[M]},$$

is the chemical loss of ozone due to oxygen chemistry,

$$L_{NO_x} = \frac{2J_{O_3}k_{11}\chi_{NO_2}}{k_2\chi_{O_2}[M]},$$

is the chemical loss of ozone due to nitrogen chemistry, and the final term in equation (1) is the transport of ozone. Furthermore, χ_q is the mixing ratio and J_q is the photolysis rate of chemical species q . The quantity k_n denotes the reaction rate of reaction n , \bar{w}^* is the stratospheric upwelling velocity, and $[M]$ is the number density (number of molecules per unit volume) for all molecules in air at a given altitude.

There is only one known reaction that provides a source of ozone in the stratosphere.

This reaction is



This reaction consumes a diatomic oxygen molecule and a ground-state monatomic oxygen molecule in the presence of an inert species³ M to produce ozone. The additional molecule M is not consumed in the reaction. The variable k_2 is called the *rate constant* of the reaction

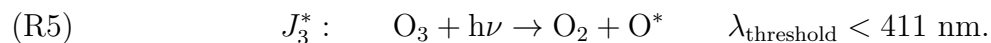
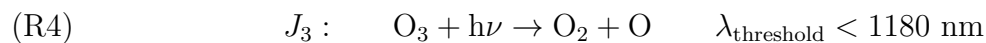
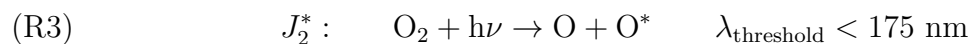
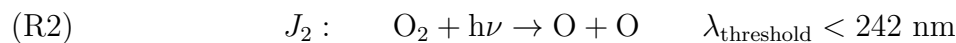
³These are also often referred to as “third-body” molecules, but in some cases this terminology is not precise since it may only be the second molecule in a reaction (see reaction R6 below). Often, the inert molecule is either a molecule of diatomic nitrogen or diatomic oxygen, since these are the most common chemicals in the atmosphere. It may also seem inaccurate to refer to diatomic oxygen as an inert molecule in the reaction above R1 since the reaction requires the consumption of diatomic oxygen, but this inert molecule or third body is merely required to absorb the energy of the reaction and does not go through any chemistry of its own (at least, none that are related to the pure oxygen chemistry of ozone).

and is used to compute the rate of the reaction as

$$(2) \quad \left(\frac{d[\text{O}_3]}{dt} \right)_{R1} = k_2[\text{O}_2][\text{O}][\text{M}],$$

where $[\text{O}_2]$, $[\text{O}]$, and $[\text{M}]$ refer to the concentrations of diatomic oxygen, monatomic oxygen, and inert molecules.

The monatomic oxygen that is used in reaction R1 can be produced through any of the following reactions



These reactions are called photolysis reactions because they each require a photon (represented by $h\nu$) to proceed. The photons involved in these reactions are all short wavelength, high energy photons from solar radiation, and the wavelengths of photons required are denoted by the $\lambda_{\text{threshold}}$ inequality to the right of each equation. Similar to the computation of the rate of reaction R1 by equation 2, the rate of a photolysis reaction such as reaction R2 is given by

$$(3) \quad \left(\frac{d[\text{O}]}{dt} \right)_{R2} = 2J_2[\text{O}_2].$$

Two of the reactions above (reactions R3 and R5) produce monatomic oxygen in the excited state (and correspondingly require higher-energy photons). This excited monatomic oxygen is transitioned into its ground state by



This reaction happens very rapidly below the mesosphere.

In addition to reaction R1, monatomic oxygen can be removed from the atmosphere through



With these reactions and those above, we have a complete description of the pure oxygen chemistry of ozone. By computing the time rate of change of each reaction (as in equations 2 and 3), we can form a system of ordinary differential equations describing the time tendency

of the concentration of each chemical, as follows.

$$\begin{aligned}\frac{d[\text{O}]}{dt} &= 2J_2[\text{O}_2] + J_2^*[\text{O}_2] + J_3[\text{O}_3] + k_4[\text{O}^*][\text{M}] \\ &\quad - 2k_1[\text{M}][\text{O}]^2 - k_2[\text{O}][\text{O}_2][\text{M}] - k_3[\text{O}_3][\text{O}] - k_6[\text{O}][\text{O}^*] \\ \frac{d[\text{O}^*]}{dt} &= J_3^*[\text{O}_3] + J_2^*[\text{O}_2] - k_4[\text{O}^*][\text{M}] - k_5[\text{O}_3][\text{O}^*] - k_6[\text{O}][\text{O}^*] \\ \frac{d[\text{O}_3]}{dt} &= k_2[\text{O}_2][\text{O}][\text{M}] - k_3[\text{O}_3][\text{O}] - k_5[\text{O}_3][\text{O}^*] - (J_3 + J_3^*)[\text{O}_3].\end{aligned}$$

A time tendency equation for diatomic oxygen can also be constructed, but this is unnecessary because this species has, to a good approximation, a fixed and uniform mixing ratio. We can also simplify the time-tendency equations for O and O* by removing minor terms so that

$$\begin{aligned}\frac{d[\text{O}]}{dt} &= J_3[\text{O}_3] + k_4[\text{O}^*][\text{M}] - k_2[\text{O}][\text{O}_2][\text{M}] \\ \frac{d[\text{O}^*]}{dt} &= J_3^*[\text{O}_3] - k_4[\text{O}^*][\text{M}].\end{aligned}$$

We then note that because the chemical timescales for these species are so short at the levels we are considering, we can assume steady state for O and O* so that the time tendencies for each species are zero. Therefore

$$\frac{d[\text{O}^*]}{dt} \approx 0 \implies [\text{O}^*] \approx \frac{J_3^*[\text{O}_3]}{k_4[\text{M}]},$$

and

$$\frac{d[\text{O}]}{dt} \approx 0 \implies [\text{O}] \approx \frac{J_3[\text{O}_3] + k_4[\text{O}^*][\text{M}]}{k_2[\text{O}_2][\text{M}]}.$$

Combination of these gives

$$[\text{O}] \approx \frac{(J_3 + J_3^*)[\text{O}_3]}{k_2[\text{O}_2][\text{M}]}.$$

To simplify the expression of the rate of change of ozone, it is also standard to define the “odd-oxygen” family of chemical, labeled by O_x , so that

$$(4) \quad [\text{O}_x] = [\text{O}] + [\text{O}^*] + [\text{O}_3],$$

and we can also write the time tendency of this quantity as

$$(5) \quad \frac{d[\text{O}_x]}{dt} = 2(J_2 + J_2^*)[\text{O}_2] - 2k_1[\text{O}]^2[\text{M}] - 2k_3[\text{O}_3][\text{O}] - 2k_5[\text{O}^*][\text{O}_3] - 2k_6[\text{O}^*][\text{O}],$$

which allows us to remove terms from the time tendency equation that represent a chemical change from one odd-oxygen species to another.

This definition becomes very useful when we observe that for altitude below the mesosphere it is a very good approximation that $\text{O}_x \approx \text{O}_3$. Therefore we can approximate

$$\frac{d[\text{O}_x]}{dt} \approx \frac{d[\text{O}_3]}{dt},$$

and by applying this approximation and neglecting minor terms of Equation 5 (Brasseur and Solomon [4]) we find that

$$(6) \quad \frac{d[\text{O}_3]}{dt} = 2(J_2 + J_2^*)[\text{O}_2] - 2k_3[\text{O}_3][\text{O}],$$

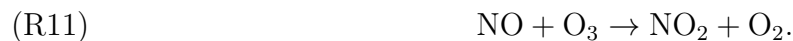
which means that

$$\frac{d[\text{O}_3]}{dt} = 2(J_2 + J_2^*)[\text{O}_2] - \frac{2(J_3 + J_3^*)k_3}{k_2[\text{O}_2][\text{M}]}[\text{O}_3]^2,$$

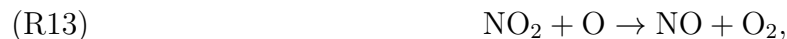
by substitution of our expression for steady-state O. To simplify the descriptions to follow, we define $J_{\text{O}_2} = J_2 + J_2^*$ and $J_{\text{O}_3} = J_3 + J_3^*$. Therefore

$$(7) \quad \frac{d[\text{O}_3]}{dt} = 2J_{\text{O}_2}[\text{O}_2] - \frac{2J_{\text{O}_3}k_3}{k_2[\text{O}_2][\text{M}]}[\text{O}_3]^2.$$

As mentioned at the beginning of this section, pure oxygen chemistry is not sufficient to capture the behavior of the chemical sink of ozone. But, in the absence of aerosols the catalytic cycles of ozone destruction by nitrogen species can supplement pure oxygen chemistry to provide a sufficient chemical sink of ozone. The relevant nitrogen species for this are NO and NO₂. In the stratosphere, these exchange rapidly by the reactions



These reactions result in no change in total nitrogen species amounts. Similarly, because the first reaction consumes an ozone molecule and the latter produces a monatomic oxygen molecule, there is no change in odd-oxygen amounts. However, another reaction



removes odd-oxygen from the atmosphere. The rate of odd-oxygen destruction by nitrogen is then given by

$$\frac{d[\text{O}_3]}{dt} = 2k_{11}[\text{NO}_2][\text{O}] = \frac{2k_{11}[\text{NO}_2]J_{\text{O}_3}[\text{O}_3]}{k_2[\text{O}_2][\text{M}]},$$

where $[O]$ is given by the previously used steady-state approximation. The total chemical change of ozone in this model is therefore given by

$$\frac{d[O_3]}{dt} = 2J_{O_2}[O_2] - \frac{2J_{O_3}k_3}{k_2[O_2][M]}[O_3]^2 - \frac{2J_{O_3}k_{11}[NO_2]}{k_2[O_2][M]}[O_3]$$

A final process that must be added to produce the terms of the full continuity equation (1) is the vertical transport of ozone. Given a profile of ozone $[O_3](z)$ and a profile of upwelling $\bar{w}^*(z)$, the change in ozone over time due to transport is

$$(8) \quad \left(\frac{d[O_3]}{dt}(z) \right)_{transport} = -\bar{w}^*(z) \frac{\partial[O_3]}{\partial z}(z),$$

so that

$$\frac{d[O_3]}{dt} = 2J_{O_2}[O_2] - \frac{2J_{O_3}k_3}{k_2[O_2][M]}[O_3]^2 - \frac{2J_{O_3}k_{11}[NO_2]}{k_2[O_2][M]}[O_3] - \bar{w}^* \frac{\partial[O_3]}{\partial z}.$$

A final change that must be noted is that for a chemical q the concentration $[q]$ is equal to $\chi_q[M]$. Therefore

$$\frac{d[O_3]}{dt} \approx [M] \frac{d\chi_{O_3}}{dt} = 2J_{O_2}\chi_{O_2}[M] - \frac{2J_{O_3}k_3}{k_2\chi_{O_2}[M]}\chi_{O_3}^2[M] - \frac{2J_{O_3}k_{11}\chi_{NO_2}}{k_2\chi_{O_2}[M]}\chi_{O_3}[M] - \bar{w}^* \frac{\partial\chi_{O_3}}{\partial z}[M],$$

so that

$$\frac{d\chi_{O_3}}{dt} = 2J_{O_2}\chi_{O_2}[M] - \frac{2J_{O_3}k_3}{k_2\chi_{O_2}[M]}\chi_{O_3}^2 - \frac{2J_{O_3}k_{11}\chi_{NO_2}}{k_2\chi_{O_2}[M]}\chi_{O_3} - \bar{w}^* \frac{\partial\chi_{O_3}}{\partial z},$$

which is equivalent to equation (1). In this, we have neglected the change in $[M]$ in time in our model. This is acceptable because this quantity does not change rapidly when the profile is at equilibrium.

To implement this equation, we compute each of J_{O_2} , J_{O_3} , k_2 , k_3 , k_{11} , and $[M]$ on every time step. The mixing ratio of diatomic oxygen χ_{O_2} is taken as the observed 0.21 ppv while the mixing ratio of nitrous oxide χ_{NO_2} is taken from the reference profile provided in (Brasseur and Solomon [4]).

The value of $[M]$ is computed through the ideal gas equation because it is simply the concentration (molecules per unit volume) of all species in the atmosphere as a whole. Precisely

$$[M] = A_v \frac{P}{RT m_{air}},$$

where A_v is Avogadro's number, P is pressure, R is the ideal gas constant for air, and m_{air} is the molar mass of air.

The rate constants k_2 and k_3 are calculated from the formulas given in JPL data evaluation 18 (cite it!), a standard resource for chemistry calculations. Precisely, these expressions are $k_2(T) = 6E - 34(T/300)^{2.4}$ molecules² per cm⁶ per second, $k_3(T) = 8E - 12 \exp[-2060/T]$ molecules per cm³ per second, and $k_{11}(T) = 5E - 12 \exp[210/T]$ molecules per cm³ per second, where T is temperature.

The values of J_{O_2} and J_{O_3} require some care in calculation and are the most computationally intensive element of the ozone calculations. These photolysis rates depend strongly on altitude (monotonically increasing with height), and are calculated by

$$J(z) = \int \Phi(\lambda) \sigma(\lambda) F(z, \lambda) d\lambda,$$

or

$$(9) \quad J(z) = \int \Phi(\lambda) \sigma(\lambda) F_0(\lambda) Tr(z, \lambda) d\lambda,$$

where $\sigma(\lambda)$ is the wavelength-dependent absorption cross-section, Φ is the quantum yield, and $F(z, \lambda)$ is the actinic flux, $F_0(\lambda)$ is the top-of-model actinic flux, and $Tr(z, \lambda)$ is the atmospheric transmission function. While these equations are equivalent, we only use the latter form in this work, although the computation of J_{O_2} requires a parameterization that breaks from this form. Because of that, the computation of J_{O_3} is considerably simpler and so we will begin by discussing its computation first.

The quantum yield $\Phi(\lambda)$ is the number of molecules produced by the results of the impact of a single photon, and is generally a number between (or including) 0 and 1. For computation of J_3 and J_3^* the quantum yield is not 1 and (for some wavelengths) depends on temperature. However, we wish to compute $J_{O_3} = J_3 + J_3^*$, and to the knowledge of the author (Atkinson et al. [1]), the sum of the quantum yields for J_3 and J_3^* is 1, and therefore the quantum yield for J_{O_3} is 1.

Next, the cross-sections depend strongly on wavelength and may also depend on temperature and pressure. For the computation of J_{O_3} , the cross-sections do not depend strongly on pressure but do depend somewhat on temperature, but only for a particular range of wavelengths. This dependence is also rather small, and so for the present work we have neglected the dependence on temperature. The cross-section data we use are the recommended data from JPL data evaluation 18 [6].

The top-of-atmosphere actinic flux, which we have obtained from WMO Report No. 16 [18], can be used to compute the top-of-model actinic flux $F_0(\lambda)$. While these two quantities are very similar, consistency is desirable and the calculation to obtain $F_0(\lambda)$ from the top-of-atmosphere actinic flux is straightforward. To do this, we compute the model-top to

atmosphere-top transmission function $Tr_{top}(\lambda)$. This is computed by

$$\begin{aligned} Tr_{top}(\lambda) &= Tr_{top,O_2}(\lambda)Tr_{top,O_3}(\lambda) \\ &= \exp[-\sigma_{O_2}(\lambda)O_{2,TOM-column} \cos(\theta)^{-1}] \exp[-\sigma_{O_3}(\lambda)O_{3,TOM-column} \cos(\theta)^{-1}], \end{aligned}$$

where the subscript *TOM-column* indicates that the chemical variable is the total column of the chemical (that is, the number of molecules overhead per unit area) and θ is the solar zenith angle. Calculating $O_{2,TOM-column}$ merely requires computing the total mass of the atmosphere above the model by converting the top-of-model pressure to the mass of atmosphere above the model, multiplying by the constant, vertically-uniform mass mixing ratio of diatomic oxygen, and then converting this value into number of molecules. Calculating $O_{3,TOM-column}$ cannot be done in such a clean way because ozone is not constant with height, but an approximate reference value for above-model total column ozone was obtained from Brausser and Solomon which suffices for this study. With the number that results from this, we can compute the top-of-model actinic flux by $F_0(\lambda) = F_{TOA}(\lambda)Tr_{top}(\lambda)$.

The transmission function, $Tr(z, \lambda)$, is computed in essentially the same way as $Tr_{top}(\lambda)$ above. Precisely,

$$\begin{aligned} Tr(z, \lambda) &= Tr_{O_2}(z, \lambda)Tr_{O_3}(z, \lambda) \\ &= \exp\left(-\int_z^\infty \sigma_{O_2}(z', \lambda)\chi_{O_2}[M](z')dz' \cos(\theta)^{-1}\right) \exp(-\sigma_{O_3}(\lambda)O_{3,column}(z) \cos(\theta)^{-1}), \end{aligned}$$

where $O_{3,column}(z)$ is the overhead column of ozone at altitude z . Note that the cross-sections for diatomic oxygen depend on altitude while those for ozone do not because of the pressure

dependence of diatomic oxygen cross-sections. This is because the diatomic oxygen cross-sections depend on pressure (Yoshino et al. [19]), as discussed in the description of the J_{O_2} computation. With this and the other calculations described above, J_{O_3} is computed on every time step by integrating these values over the wavelength range 200 nm - 827.5 nm. These boundaries are chosen because they are the lower and upper limits of wavelengths for which JPL data evaluation 18 [6] provides ozone cross-section data.

The computation of J_{O_2} is more complicated than the calculation of J_{O_3} in that there is substantially different behavior in J_{O_2} at wavelengths above and below about 205 nm. The wavelengths below 205 nm and above 175 nm are referred to as the Schumann-Runge Bands⁴ while the spectrum above 205 nm and below 245 nm is referred to as the Herzberg continuum.

The Herzberg continuum contribution to J_{O_2} is relatively straightforward to compute, and the methods of computation for this region are the same as described for the computation of J_{O_3} except that the cross-sections for diatomic oxygen in equation 9 depend linearly on pressure (Yoshino et al. [19]). For the computation of J_{O_2} in the Herzberg continuum, the quantum yield is 1 as suggested by JPL data evaluation 18 [6], the cross-sections are given by Yoshino et al. [19] (as recommended by JPL data evaluation 18 [6]), and the top-of-atmosphere actinic flux is given by WMO Report No. 16 [18].

The Schumann-Runge continuum presents a special case because the cross-sections of diatomic oxygen in this range require very high resolution (with respect to wavelength) data to be represented appropriately, whereas the cross-sections described elsewhere in this work

⁴There is also a feature in the diatomic oxygen cross-section spectrum called the Schumann-Runge continuum that overlaps with the Schumann-Runge bands. While some studies distinguish between the continuum and the bands, the continuum is not significant below 80 km and so the work of this study falls well within the bounds where it can be reasonably ignored, and so the Schumann-Runge continuum is not computed here.

change much more gradually over wavelength and are therefore well-represented by a relatively small number of wavelength bins. This high-resolution information can become very computationally intensive, so a large number of parameterizations have been developed to ease the computational burden of the Schumann-Runge bands. For this work, the parameterization of Minschwaner et al. 1993 [14] is used. The fundamental change in this is that equation 9 has a different form that approximates the Schumann-Runge bands well. By computing this parameterization along with computing the photolysis contribution of the Herzberg continuum, the photolysis rate for diatomic oxygen J_{O_2} is computed. This is the final variable required to compute the rate of change of ozone due to chemistry, and thereby we have established a simple scheme to predict ozone concentrations.

However, the limitations of our model require one more process to be included. This is that ozone concentrations are prevented from reducing below a minimum value (this is 40 ppbv - approximately the tropospheric concentration seen in the SHADOZ dataset). This must be enforced because the chemistry outlined in this model does not incorporate the tropospheric chemistry of ozone and therefore the chemical source of ozone in the troposphere could otherwise result in arbitrarily low ozone concentrations. This process is similar to the convective adjustment scheme for temperature changes. In particular, convective adjustment instantly fixes low temperatures to a higher temperature based on a fixed tropospheric property, while this tropospheric ozone mechanism instantly brings low ozone mixing ratios up to a specified tropospheric value.

We wish to note about the use of two separate radiative transfer methods for the two major components of this model. In the case of temperature, the RRTMG model is used to compute heating rates, the theory of which is based on the correlated-k approximation

to radiative transfer. The ozone computations, meanwhile, use a standard interpretation of radiation transmission that is based in well-established radiation theory without substantial approximation. One might note that this represents an inconsistency in the methods of this work. However, only a few modern climate-chemistry models utilize the same methods for radiative transfer and photolysis computations (Eyring et al. [7]), and so this inconsistency is common in these sorts of computations.

Another note is that for experts of ozone chemistry the methods used here may seem overly simple. However, as is shown in the following sections the ozone profiles this model produces when using the basic parameters of this work (e.g. 0.5 mm/s stratospheric upwelling, 6.5 K/km critical convective lapse rate) are remarkably similar to observations. The temperature profiles that result from this, as well, can be very similar to observed temperature profiles.

CHAPTER 3

RESULTS

3.1. RADIATIVE CONVECTIVE EQUILIBRIUM AND PHOTOCHEMICAL EQUILIBRIUM WITHOUT THE FULL EFFECTS OF UPWELLING

This chapter describes the important results from the use of the model described in the previous chapters. The profiles shown were produced through radiative convective equilibrium (RCE) of temperatures and photochemical equilibrium (PCE) of ozone concentrations. While “photochemical equilibrium” may be taken to imply that an ozone profile was computed exclusively through consideration of chemistry, “PCE” is also used to refer to profiles that were produced through a balance of chemistry and transport, for the sake of the simplicity of notation. The use of transport, however, will be noted for each profile for which transport was utilized. Some profiles are referred to as being RCE-PCE profiles. This indicates that simultaneous computations of RCE and PCE were performed.

Ozone concentrations in the atmosphere are only near pure photochemical equilibrium (i.e. insignificant transport) in some locations and elsewhere are in a balance between photochemistry and transport. To illustrate this, consider the right panel of Figure 3.1. In this figure, observed temperature and ozone profiles are shown alongside profiles of RCE-PCE ozone and temperature. The ozone profiles shown were produced without the use of transport, and it can be seen from these profiles that calculated ozone is very similar to observed ozone above about 30 km. Calculated ozone below 30 km, meanwhile, is substantially greater than observed ozone due to transport having been neglected in these computations. This is consistent with expectations (Solomon et al. [16]), shown in Figure 1.4, where chemical

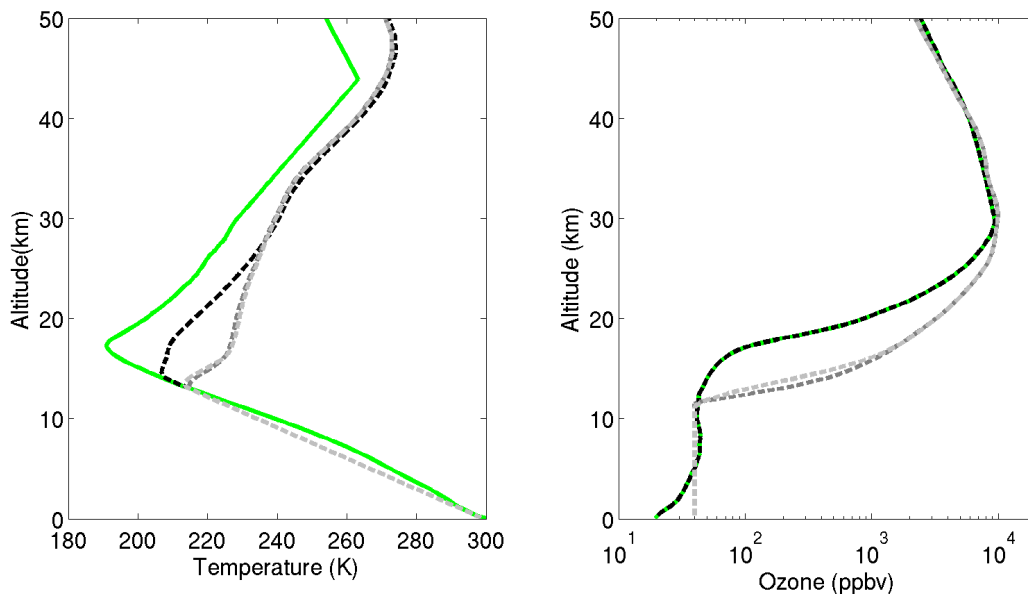


FIGURE 3.1. Profiles of temperature (left) and ozone (right). Shown are observations from SHADOZ (solid green), control run with SHADOZ ozone (dashed black), RCE-PCE computed through integration (dashed light gray), and RCE-PCE computed through the quasi-analytical method (dashed dark gray).

production and destruction are the dominant processes determining ozone concentrations above the lower stratosphere.

The two calculated profiles shown in Figure 3.1 were produced through two different methods of proceeding towards equilibrium. The “integration” profile was produced through the standard RCE method of integrating the tendency equations (e.g. heating rates, ozone chemistry) for a long simulation time. In this case, 10,000 days were simulated. While this is certainly a very long time for an RCE experiment, the chemical source and sink of ozone are not equal¹ at the end of this integration, as shown in the left panel of Figure 3.2. The chemical sink here is smaller than the source, showing that equilibrium ozone concentrations are higher than the computed values. Obtaining ozone profiles much closer to equilibrium

¹Due to the process of fixing a tropospheric minimum ozone mixing ratio, no chemical source and sink corresponding to an experiment in this work actually balance at all levels. The lower atmosphere (below 11 km) always shows a sink larger than the source, and this is because the tropospheric ozone mixing ratio is larger than the pure photochemical equilibrium value that the chemical scheme of this work obtains.

(e.g. within 1%) would then require a longer integration time. A lower bound for this length of time can be obtained by assuming that the source and sink do not change in time, giving an estimated 40 years.

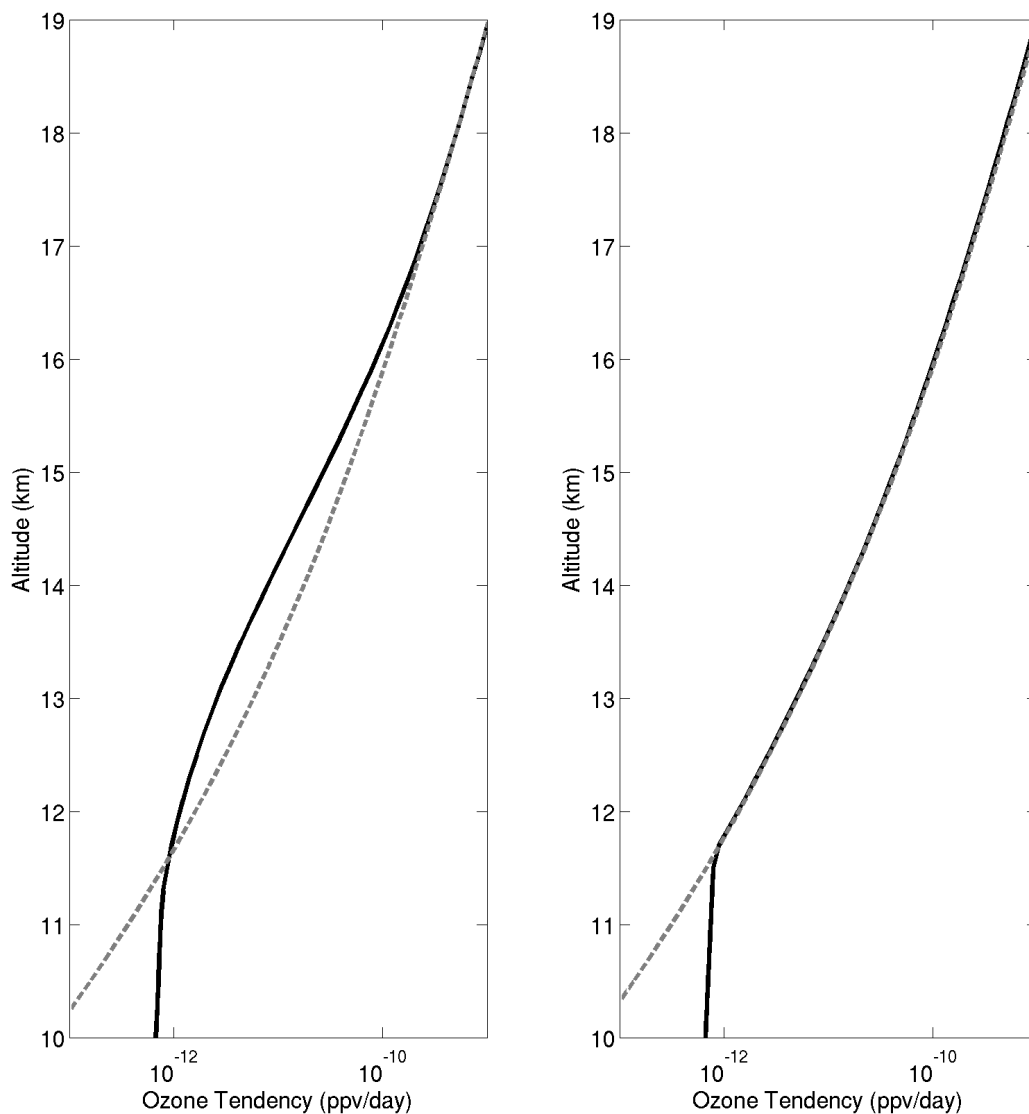


FIGURE 3.2. Daily-averaged chemical source (light dashed lines) and sink (dark solid lines) of ozone produced through integration (left) and quasi-analytical method (right).

However, an alternative, quasi-analytical, method can be applied to obtain equilibrium ozone mixing ratios. Precisely, because the chemical sinks of ozone depend explicitly on the mixing ratio of ozone, the ozone mixing ratio that balances a given source and set of sink coefficients² can be determined from the source and sink coefficients. Because the chemical terms of the ozone continuity equation, Equation 1, form a quadratic equation, the ozone mixing ratio that balances the chemical terms is given by

$$(10) \quad \chi_{\text{O}_3} = \frac{L_{\text{NO}_x}}{2L_{\text{O}_x}} + \sqrt{\left(\frac{L_{\text{NO}_x}}{2L_{\text{O}_x}}\right)^2 + \frac{P}{L_{\text{O}_x}}},$$

using the notation of Equation 1.

This profile can then be used in a RCE-PCE integration that is long enough to obtain equilibrium temperatures (500 days). The resultant source and sink terms can then be used to determine the balancing ozone profile, and if this is close enough to the integrated profile then the RCE-PCE result can be considered to be at equilibrium. If not, the process can be repeated. In practice, approximately 10 repetitions are required for the result to be within 1% of the chemical-balance estimate.

Examining the ozone profiles in Figure 3.1 shows that both quasi-analytical ozone and integrated ozone are larger than the observed ozone in the lower stratosphere but very close to observed ozone above about 30 km. The difference between PCE and observed ozone is largest at about 16.5 km and the large differences are apparent beginning at about 11.5 km and end just below 30 km, at about 28 km. This is more easily examined in Figure 3.4, where it can be seen that the largest difference between PCE and observed ozone is a factor of about 16. This also shows that the difference between integrated and quasi-analytical ozone

²That is, the sinks of ozone divided by the ozone they explicitly depend upon, whether to the first or second power.

is relatively small. In fact, this difference is only about a factor of two at most, maximizing at 13.5 km.

The larger concentrations of PCE ozone compared to observed ozone also result in a substantial increase in shortwave heating rates, shown in Figure 3.3. Near 18 km, the shortwave heating rate more than doubles, from 1.9 K/day to 4.8 K/day. At higher altitudes (above 40 km), decreases of similar magnitude in the shortwave heating rate are observed. However, these ultimately do not change RCE temperatures by much at all compared to the doubling of shortwave heating in the TTL, as can be seen in the left panel of Figure 3.1.

The largest difference between the quasi-analytical RCE-PCE temperature and the control RCE temperature is 17 K at 17 km, approximately the location of the observed cold point tropopause. At this altitude, the difference between RCE-PCE temperature and observations is nearly 35 K. Above 28 km, the RCE-PCE temperatures are less than 2 K lower than control RCE temperatures, but are always lower. The cold point tropopause is much lower and much warmer in the RCE-PCE result than in the RCE control profile, with 215 K at 13 km compared to 207 K at 15 km. The convection top is similarly lower and warmer in the RCE-PCE case than the RCE control case, with 217 K and 12.5 km versus 210 K and 14 km. This gives a TTL vertical extent of only 0.5 km - far less than the observed 5 km between the level of main convective outflow and the cold point tropopause.

These are very large temperatures, substantially larger than the control RCE profile. However, we have previously shown (in Section 2.1) that stratospheric upwelling can cause large temperature changes through adiabatic cooling. We might therefore expect that the introduction of dynamics could reduce temperatures substantially, although the large shortwave heating rates in the TTL will remain higher than the cases with observed ozone.

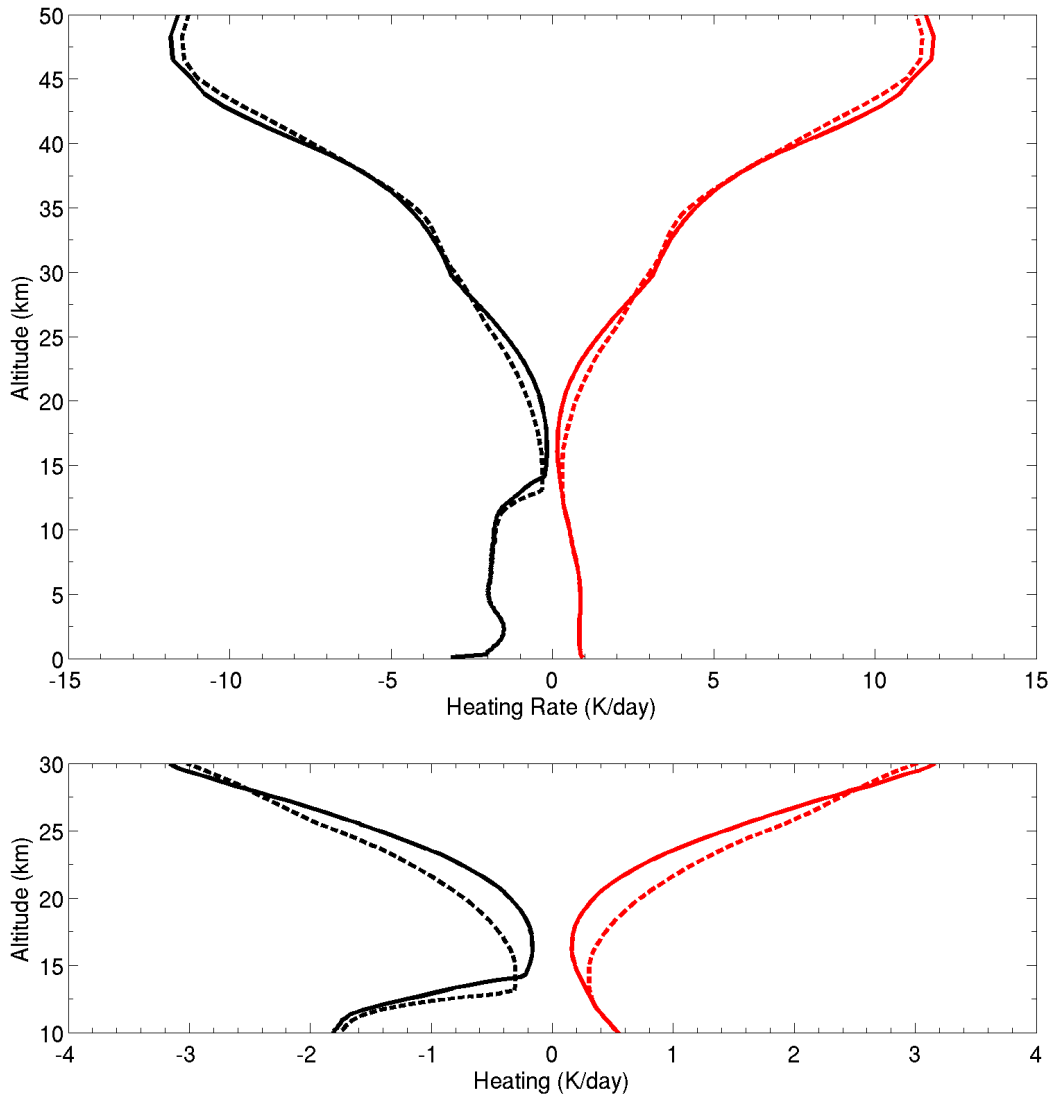


FIGURE 3.3. Shortwave (red) and longwave (black) heating rates for control run (solid lines) and quasi-analytical RCE-PCE (dashed lines). Top panel: whole profile; Bottom panel: focus on TTL region.

3.1.1. THE INTRODUCTION OF DYNAMICS ALONE. The left panel of Figure 3.5 shows an RCE-PCE profile of temperature created through the quasi-analytical method with dynamics applied through a 0.5 mm/s upwelling. The addition of dynamics does reduce equilibrium

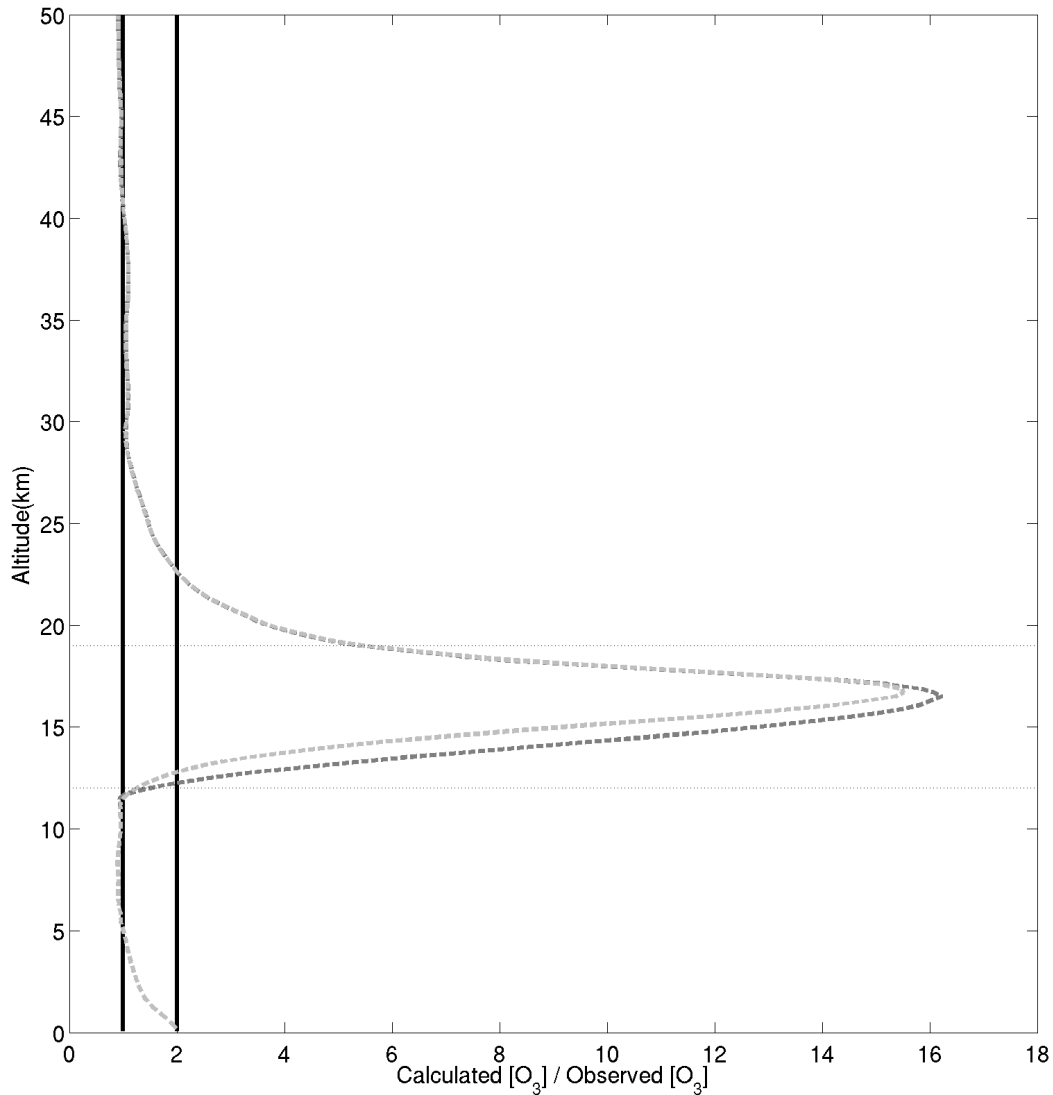


FIGURE 3.4. Fractional difference between observed ozone concentration and calculated ozone. Ozone is calculated from integration (dashed light gray line) and quasi-analytical method (dashed dark gray line). Solid black lines are present to provide a clear indication of the locations of fractional difference values of 1 and 2. Horizontal dashed lines show the lower and upper boundaries of the observed TTL.

temperatures substantially, maximizing with a cooling of 13 K at 16 km relative to the RCE-PCE profile without dynamics. The cold point is lofted and cooled from the case of RCE-PCE without dynamics to 14.5 km and 208 K over 13 km and 215 K. This cooling, however,

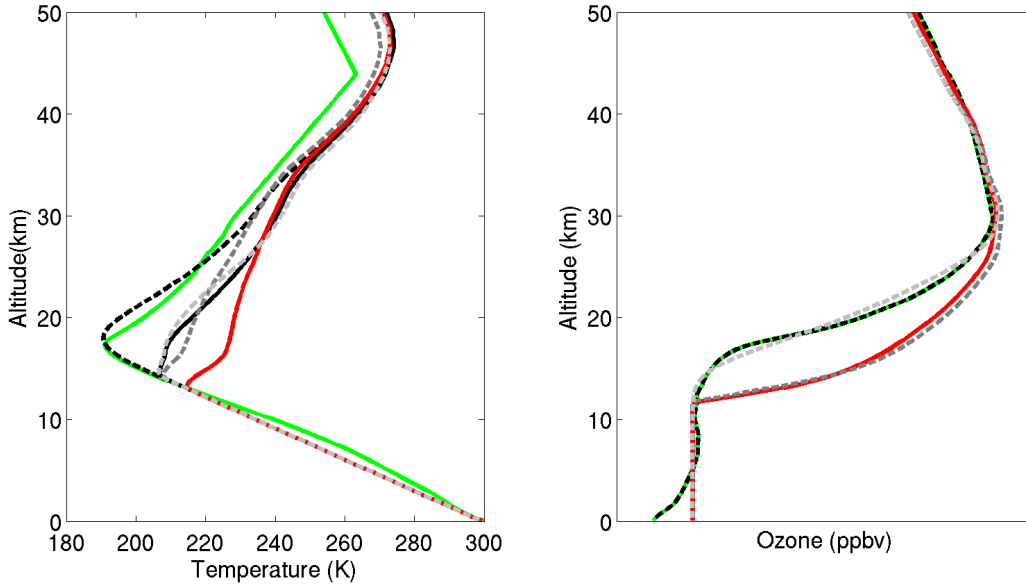


FIGURE 3.5. Equilibrium temperature and ozone profiles for computations with photochemical equilibrium ozone (solid red), RCE without dynamics and with observed ozone (solid black), RCE with dynamics and with observed ozone (dashed black), RCE-PCE with dynamics (dashed dark gray), and RCE-PCE with transport (dashed light gray). Dynamics and transport are produced through 0.5 mm/s stratospheric upwelling. Observed profiles shown for reference (solid green).

is rather limited considering that this altered temperature profile is structurally the same as the RCE-PCE profile without dynamics, showing a very rapid increase in temperature between the cold point and about 16 km and a longer range, between 16 and 30 km, where temperatures increase at a slower rate. Compared to the RCE control profile with dynamics, the RCE-PCE profile with dynamics is as much as 25 K warmer, at 18 km. Additionally, the introduction of dynamics in the case with observed ozone results in an approximate 3 km lofting and 16 K cooling of the cold point, while the introduction of dynamics with RCE-PCE ozone shows half this effect in altitude and less than half in temperature.

As expected, the high ozone concentrations in the TTL have produced a substantial barrier to the effectiveness of dynamics. The corresponding ozone profile, depicted in the right panel of Figure 3.5, shows that the inclusion of dynamics slightly increases ozone in the

middle part of the column. This occurs because the sink terms decrease as temperatures increase, due to the dependence of the sink reaction rate coefficients on temperature. In the lower part of the column, the ozone concentrations decrease due to a change in photolysis rates caused by the increased absorption of radiation in the middle column, while in the higher column, ozone concentrations decrease because the number density of air decreases due to increased temperatures, such that more monatomic oxygen follows the pathways of ozone destruction and less follows the pathway of ozone creation through Reaction R1.

The largely increased ozone in the TTL means that shortwave heating rates are stronger in some locations. This is a small effect (less than 10% change), however, and the shortwave heating is approximately that shown in Figure 3.3. This strong shortwave heating, compared to that produced through observed ozone, is too great for dynamics to overcome. That the effect of dynamics is approximately half as effective at changing the cold point in the presence of photochemical ozone as it was in the presence of observed ozone is notable, considering that the TTL shortwave heating rates are approximately twice as strong in the RCE-PCE ozone case as in the observed ozone case. For dynamics to be effective, then, either upwelling must be increased substantially or the shortwave heating rates must be reduced by the transport of ozone.

3.1.1.1. *The Introduction of Transport Alone.* Also shown in the right panel of Figure 3.5 is an RCE-PCE profile of ozone created through numerical integration with transport applied through a 0.5 mm/s upwelling. This was created through integration because the quasi-analytical method can only be applied for pure photochemical equilibrium experiments. This profile shows a substantial decrease in ozone in the TTL compared to the cases with PCE ozone in the absence of transport. In fact, this computed ozone is remarkably close to

the observations of the SHADOZ ozone data set. The difference in ozone (above the region of tropospheric ozone) compared to the observed profile maximizes at only 45% at 17.1 km. At 22 km, the calculated ozone is 28% less than observed.

This change in ozone creates shortwave heating rates that are much more similar to those of the control case, compared to the pure photochemical equilibrium ozone profile. These shortwave heating rates, below 20 km, are at most 0.01 K/day larger than the control, at 17.5 km. This corresponds to a 7% stronger heating rate over the control case. This is the most that the RCE-PCE profile is percentage-wise larger than the control, in terms of heating rates. It may be somewhat surprising then that ozone is 40% larger than the observed profile at this altitude. However, because there is so little ozone here the shortwave heating rates are more strongly determined by other species such as water.

These changes in shortwave heating rates create a structural change in the temperature profile, compared to the pure photochemical case. This is depicted in the left panel of Figure 3.5. The RCE-PCE profile is warmest compared to the control profile at 38 km, being only 2 K warmer. Between the surface and 17 km, the control profile and the transported RCE-PCE profile are only 2 K apart at the most, while above this level the largest difference is 4 K at 22 km with the RCE-PCE profile colder than the control. In fact the cold points for the transported RCE-PCE profile and the control profile are at the same model layer (15 km) and are nearly the same temperature (207 K), only 0.29 K apart, with the transported profile being colder. This is rather remarkable. Between the similar temperature, ozone profiles, and especially the similar low shortwave heating rates in the TTL it seems very likely that the introduction of dynamics to the transported RCE-PCE profile will produce results that are very similar to those of the RCE profile with applied dynamics.

3.2. THE SIMULATION WITH TRANSPORT AND DYNAMICS

Figure 3.6 shows profiles of RCE-PCE ozone and temperature with applied dynamics and transport. For the sake of brevity, these profiles will simply be referred to as the full simulation. This represents the simulation with the most realistic conditions applied in this work. The cold point for this simulation is 191 K and 18 km, just a kilometer higher than the observed cold point, but effectively at the same temperature, and the RCE-PCE cold point is at the same temperature and layer as the cold point of the RCE profile with observed ozone and dynamics. The convection top is also similar between the full simulation and the simulation of observed ozone and dynamics, with both at 204 K and 15 km. The broader profile shows full simulation temperatures colder than observed near 22 km, as is the case for the observed ozone and dynamics temperatures³. However, the TTL produced in the full simulation is qualitatively very similar to observations.

This is because the dynamics applied in the full simulation is able to effectively change temperatures in the TTL due to the low ozone concentrations there and consequent low shortwave heating rates. Conversely, the simulation with RCE-PCE ozone without applied transport showed large shortwave heating rates in the TTL, and therefore the dynamics that was applied was unable to reduce temperatures to the observed profile. This is illustrated in Figure 3.7. The dynamic heating shown here is approximately of the same magnitude (about 0.5 K/day) at 18 km, where the full simulation cold point lies, for both the full simulation and the RCE-PCE experiment with dynamics. However, without transport the ozone content at this altitude is large and the shortwave heating is consequently strong.

³This is likely due to a minimum in upwelling velocity at this altitude in the real atmosphere, whereas the upwelling simulated here is constant throughout the stratosphere. This should cause greater adiabatic cooling and ozone transport than in the real atmosphere, and could explain the lower temperatures.

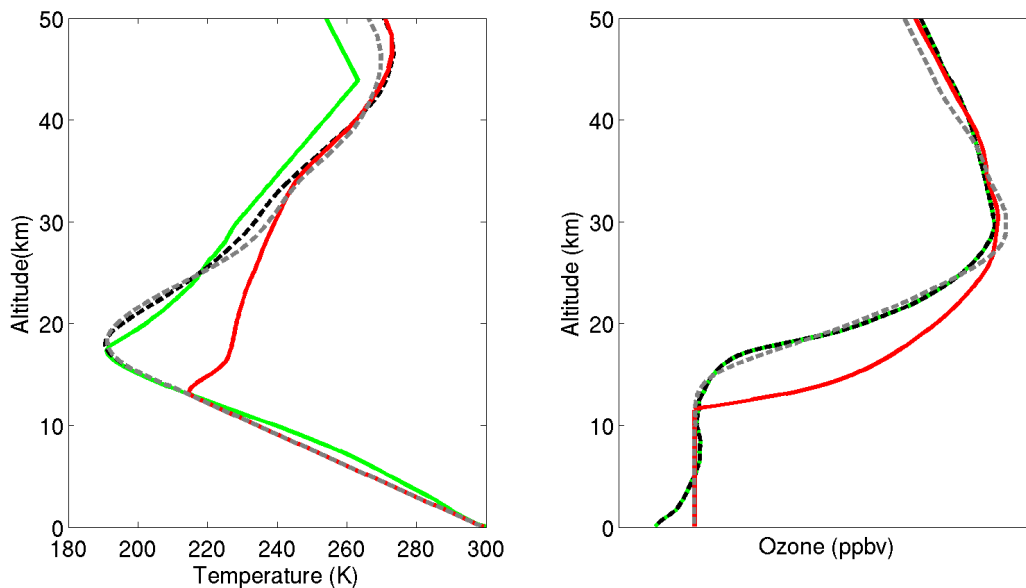


FIGURE 3.6. Profiles for temperature (left) and ozone (right). Profiles shown correspond to observations (solid green), RCE using observed ozone and dynamics (dashed black), RCE-PCE without dynamics or transport (solid red), and RCE-PCE with dynamics and transport (dashed gray). Dynamics and transport corresponding to 0.5 mm/s upwelling.

This difference can be confirmed by the right panel of Figure 3.6, where the ozone in the full simulation below 30 km is much lower than the RCE-PCE ozone. This is consistent with the result of the RCE-PCE profile with transport but without dynamics and supports the description of the ozone in this region as being in balance between transport and chemistry in the real atmosphere. The full simulation ozone also shows a consistency with the result of RCE-PCE with dynamics, in that the ozone in the middle and higher profile is larger than the RCE-PCE profile without dynamics applied. Precisely, the middle profile (near the ozone maximum at 30 km) shows increased ozone in the full simulation compared to the pure photochemical profile, while the relationship is reversed in the higher atmosphere. This supports the description of the atmosphere in this region as having an ozone balance between chemical processes alone, since the response to the temperature change seems to be

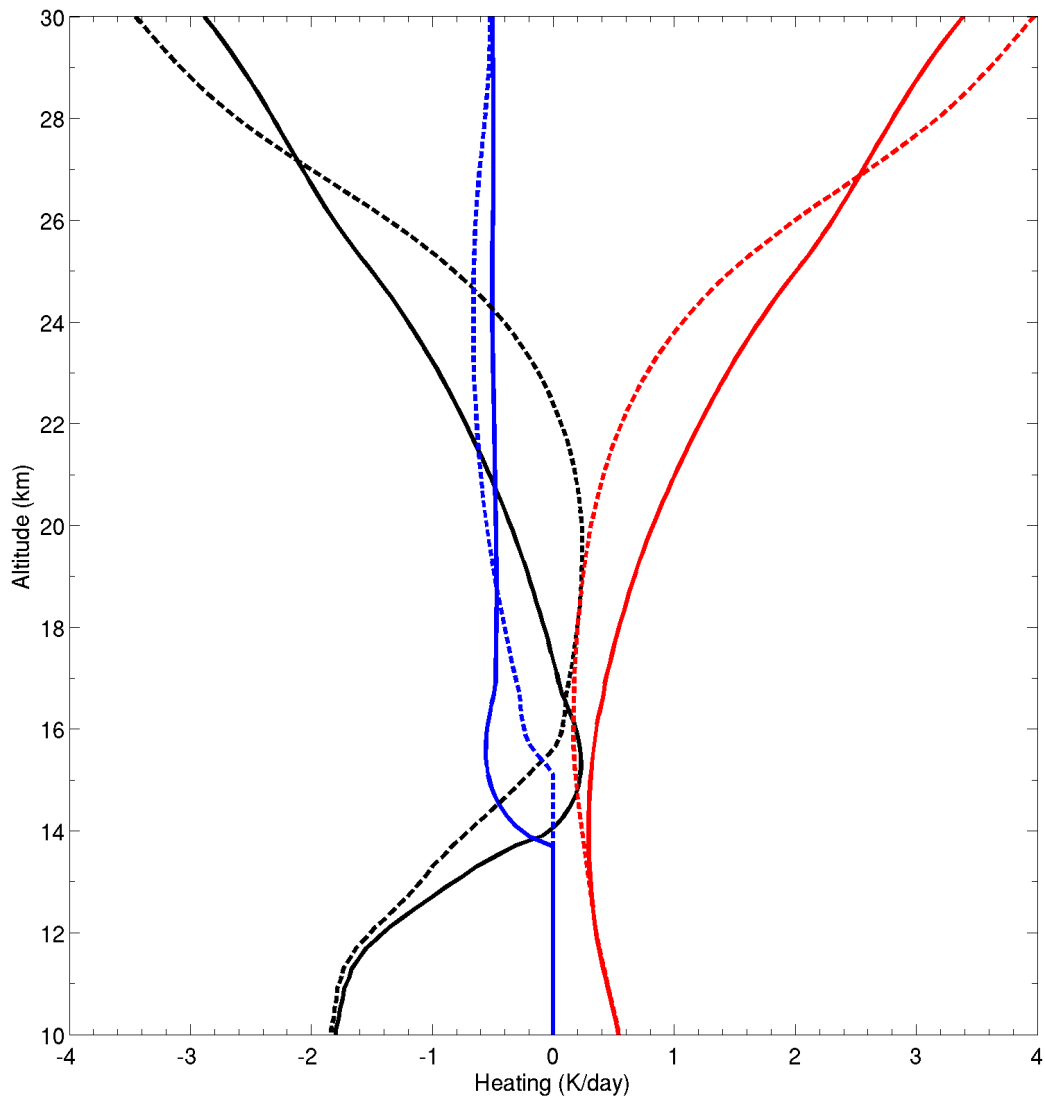


FIGURE 3.7. Heating rates from dynamics (blue profiles), shortwave radiation (red profiles), and longwave radiation (black profiles). Profiles are shown for the case of RCE-PCE ozone without transport but with dynamics (solid lines) and for the full RCE-PCE simulation with dynamics and transport (dashed lines). Dynamics and transport correspond to 0.5 mm/s upwelling.

independent of transport by similarity to the RCE-PCE profile where dynamics was applied in the absence of transport.

This is in agreement with the result of Solomon et al. [16] shown in Figure 1.4. While Solomon et al. did not suggest a precise altitude at which this transition occurs, the simplicity of this model allows for such a measure. Considering the ozone continuity equation 1, we can say that the production-transport regime exists where transport is the dominant sink term compared to chemical destruction, such that

$$\frac{d\chi_{\text{O}_3}}{dt} \approx P - \bar{w}^* \frac{\partial \chi_{\text{O}_3}}{\partial z},$$

in this regime. Therefore ozone mixing ratios at equilibrium at these altitudes should be given by

$$\chi_{\text{O}_3}(z) \approx \frac{1}{\bar{w}^*} \int_0^z P(z') dz' + \chi_{\text{O}_3,0},$$

where $\chi_{\text{O}_3,0}$ is the tropospheric minimum ozone concentration. Similarly, the continuity equation for the production-destruction regime gives that transport is negligible and so Equation 10, as used for an estimate in the quasi-analytical method, describes the RCE-PCE ozone in this regime. These predicted ozone concentrations for each regime can be calculated for the entire column, and by comparing how well each approximation predicts calculated ozone at each altitude we can suggest where the regimes exist. This comparison is shown for the full simulation in Figure 3.8.

In this figure the two predictions intersect in the troposphere, just under 10 km, and in the stratosphere at 27 km. The former intersection is simply the height where neither method produces an ozone prediction that is significantly larger than the tropospheric minimum ozone concentration. Above this intersection the production-destruction approximation shows ozone increasing rapidly with height while the production-transport approximation follows the calculated ozone profile very closely, up until about 23 km.

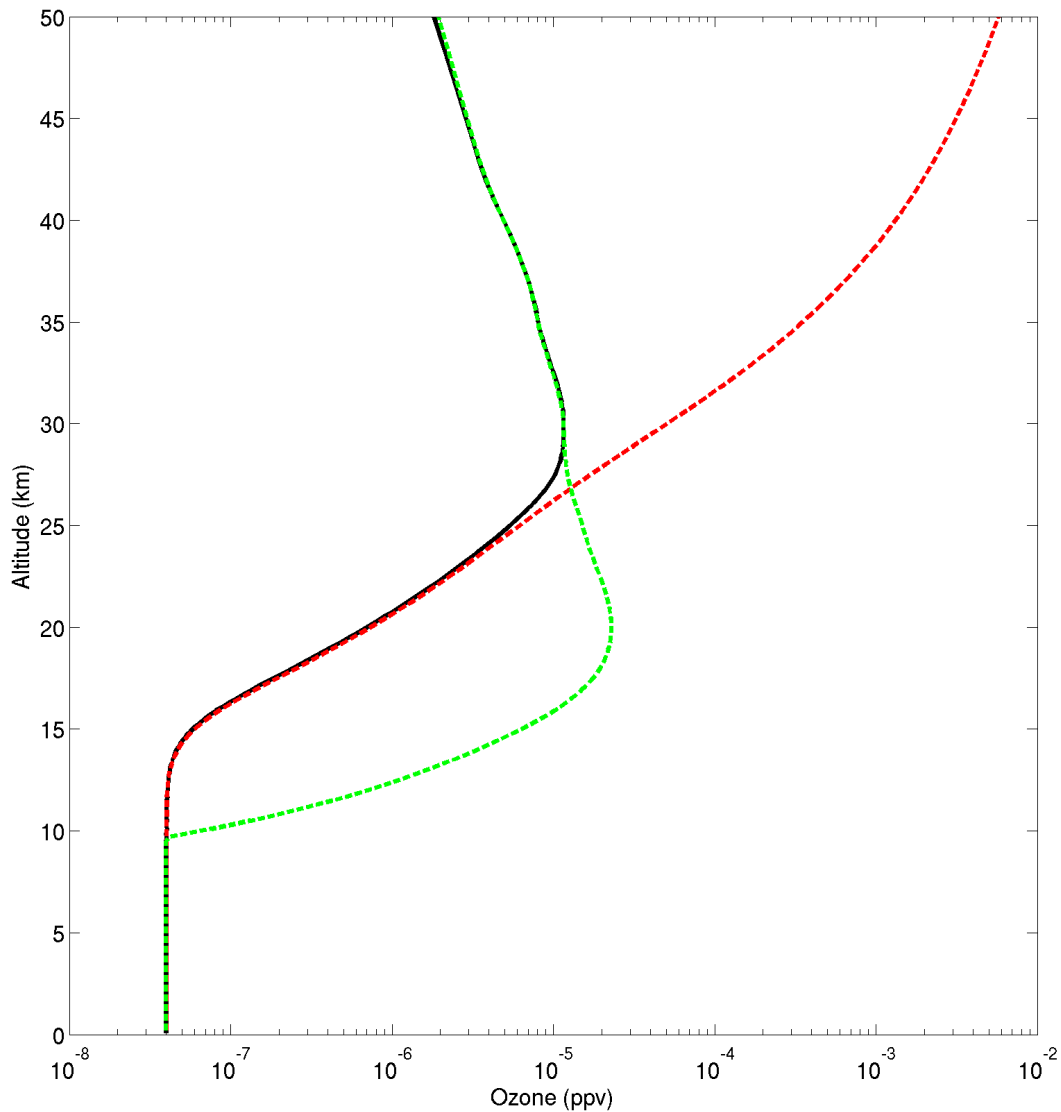


FIGURE 3.8. Example of ozone regimes for the full RCE-PCE simulation. Shown are computed ozone (solid black), production-transport balance prediction (dashed red), and production-destruction balance prediction (dashed green). The two predictions intersect at 27 km.

At 27 km, the higher intersection of the two predictions, the relationship changes so that the production-transport approximation shows ozone continuing to increase with height while the production-destruction approximation shows ozone decreasing with height, in agreement with the calculated ozone profile. We therefore say that this measure suggests 27 km as

regime transition altitude. This is in approximate agreement with the results of Solomon et al. [16]. At this level, chemical losses account for 64% of the sink of ozone while transport accounts for the remaining 36% of the sink.

Because of the computational efficiency of this model it is possible to compute these losses and sinks over a large range of \bar{w}^* values. The top panel of Figure 3.9 shows the results of doing so, ranging \bar{w}^* from 50 times less to 20 times larger than than the approximate observed value⁴. The difference between the chemical loss and chemical production in this plot is the rate of ozone removal by transport. As upwelling increases, transport becomes increasingly important. At upwelling velocities below 0.1 mm/s, the loss appears to account for all ozone destruction at this altitude, while at the maximum upwelling shown the loss accounts for only 2% of ozone destruction. Examining the bottom panel of this figure shows the relative source and sink at 18 km, the location of the cold point in the full simulation under 0.5 mm/s upwelling. Here the chemical sink is never dominant over transport, accounting for only 10% of the loss of ozone at the lowest upwelling velocity of 0.01 mm/s. An interesting feature exists at just below 0.1 mm/s, where the change in the chemical loss tendency appears to cease decreasing briefly and then resume decreasing at a slower rate for faster upwelling velocities. It appears that this upwelling velocity is an important value, and perhaps a change occurs with respect to the extent to which transport can reduce ozone at 18 km.

3.3. THE SENSITIVITY TO CLIMATE CHANGE

The transition altitude can also be calculated for this range of stratospheric upwelling values, as well as the calculated ozone at each transition altitude. This sensitivity can suggest

⁴Computations were also performed for stratospheric upwelling values of as low as 10 picometers per seconds. However, values in between this and 0.01 mm/s were not clearly at equilibrium. It is possible that another quasi-analytical method could be utilized to reduce the required computation times of these experiments, but these low values are of less interest to the present work and so they have not been included.

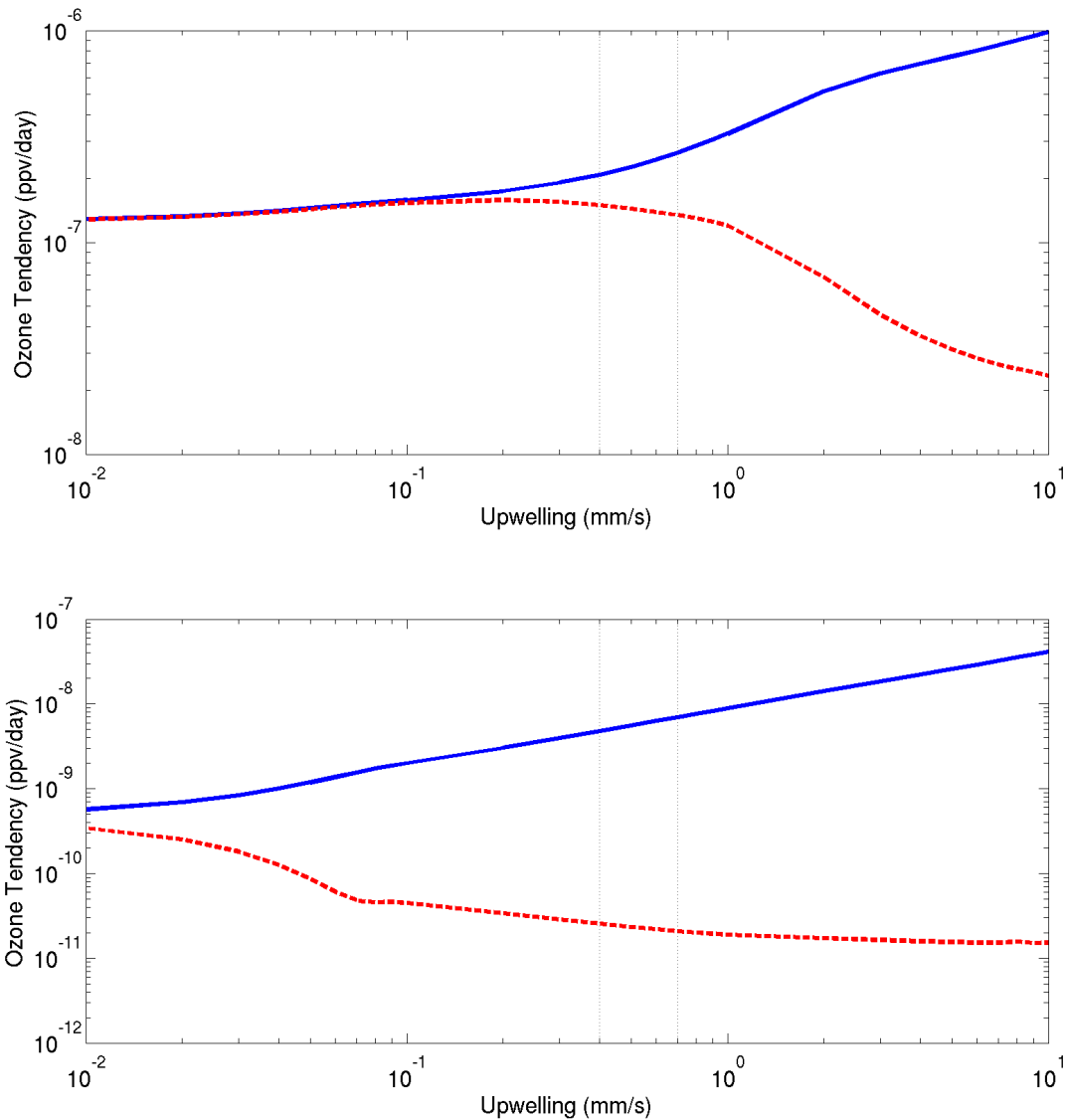


FIGURE 3.9. Equilibrium chemical source (blue) and chemical sink (dashed red) at the calculated transition altitude of 27 km (top panel) and full simulation calculated cold point of 18 km (bottom panel), calculated for the full RCE-PCE simulation with dynamics and transport of varying upwelling. The dotted vertical lines show the approximate bounds of observed upwelling.

the influence of climate change on the transition altitude, especially for the higher-than-observed upwelling velocities since the Brewer Dobson circulation is expected to strengthen due to climate change. These results are show in Figure 3.10. The relationship between the

transition altitude and stratospheric upwelling clearly shows a logarithmic response, even for the extremely large stratospheric upwelling values. However, for calculated ozone at the transition, the response appears to be logarithmic for upwelling values less than about 3 mm/s while the relationship breaks down for faster upwelling velocities. The upwelling velocity at which this relationship breaks down appears to be just faster than the upwelling velocity that pushes the transition altitude above 30 km, where the observed ozone maximum occurs.

Additional quantities that can be calculated as upwelling increases are the altitudes and temperatures of the cold point, shown in Figure 3.11, and the convection top, shown in Figure 3.12, as well as the broad properties of the TTL such as vertical width and difference in temperature between the convection top and cold point, shown in figure (3.13).

At low upwelling velocities the most important effect of upwelling seems to be transport, given that the cold point and convection top temperatures and altitudes computed through the interaction of chemistry and transport alone are very similar to the values computed through the full model, with chemistry, transport, and dynamics included. The values produced through chemistry and dynamics, meanwhile, consistently give warmer and lower cold points and convection tops and do not show substantial change until approximately 0.1 mm/s. The change in the cold point and convection top at these low velocities for the case with dynamics and observed ozone also suggests that dynamics are not very effective when upwelling is slow, since the changes in cold point and convection top properties for this case are so small below 0.1 mm/s.

These results suggest that upwelling slower than about 0.1 mm/s is unable to substantially change the temperature profile through dynamics - even if transport is active - but

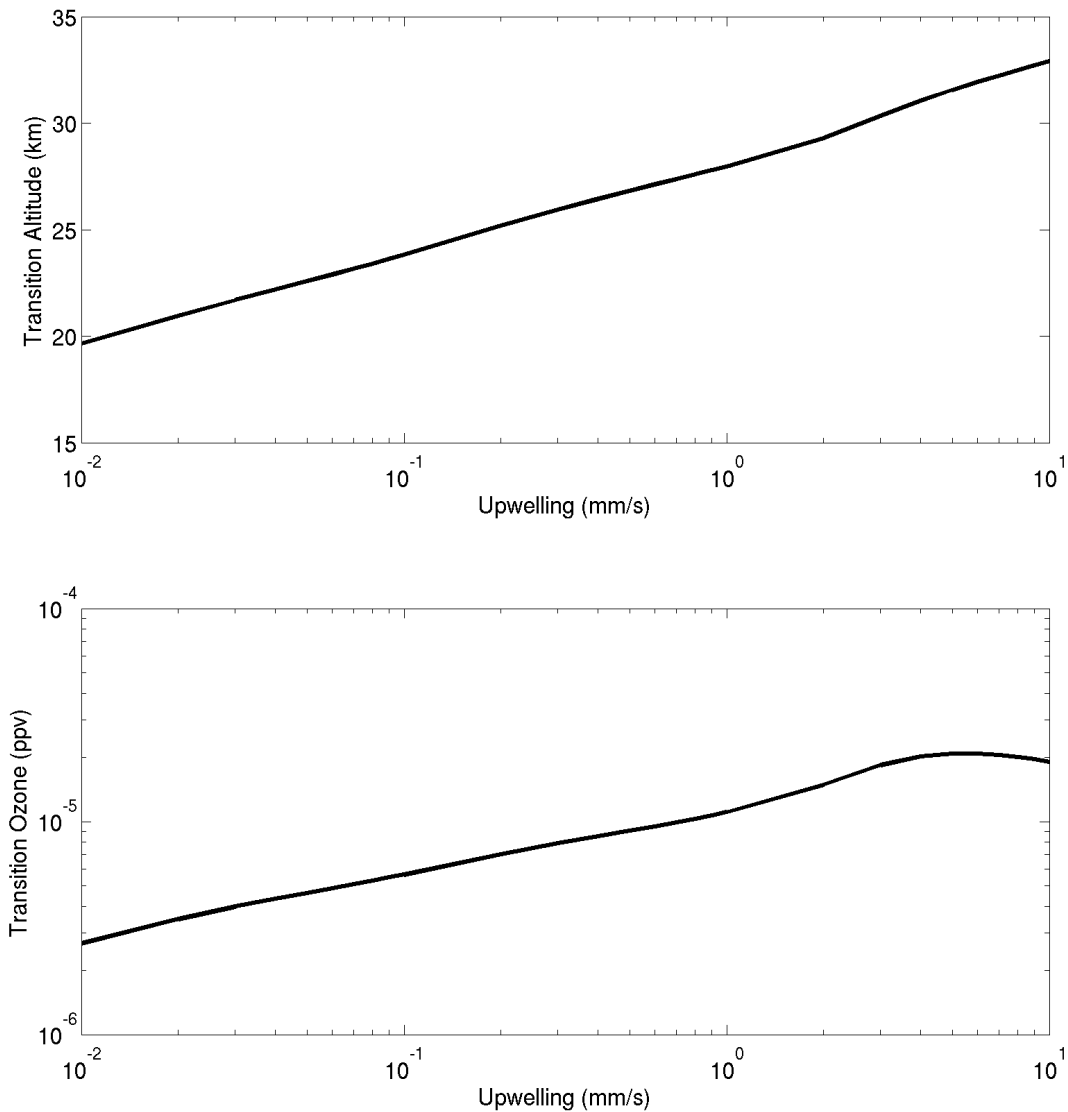


FIGURE 3.10. Ozone regime transition quantities as a function of upwelling. Top: transition altitude; Bottom: calculated ozone at transition altitude.

even upwelling of 0.07 mm/s or less is able to affect temperatures by the removal of ozone, and shortwave heating, through transport. This velocity coincides with the value noted in the discussion of the bottom panel of Figure 3.9, supporting the suggestion that upwelling velocities faster than about 0.07 mm/s do not remove substantially more ozone by transport. Further support is lent by the observation that the cold point and convection top properties

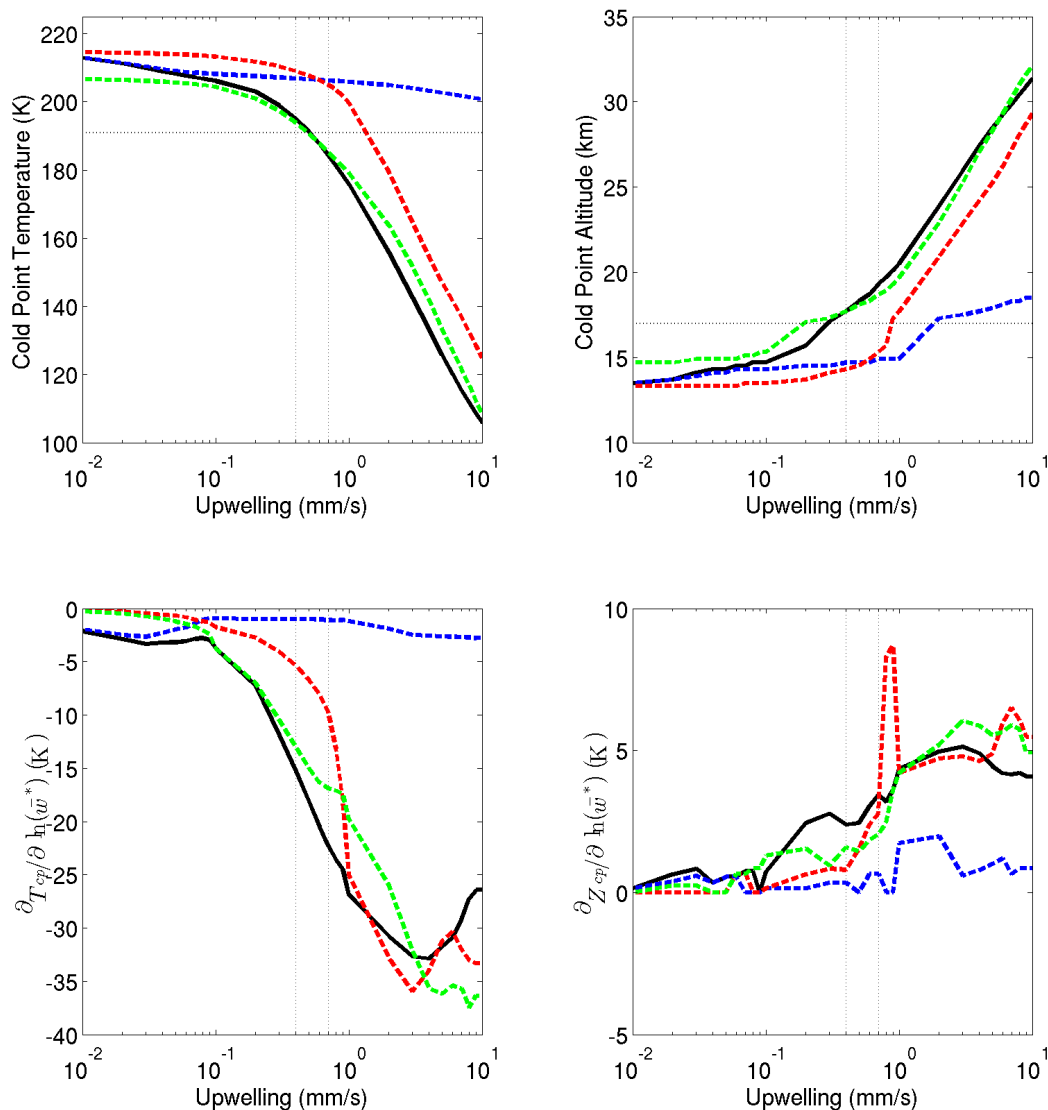


FIGURE 3.11. Cold point quantities versus stratospheric upwelling for RCE profile computed with SHADOZ ozone and dynamics (green dashed), photochemistry with transport and dynamics (solid black), photochemistry with only dynamics (dashed red), and photochemistry with only transport (dashed blue). Upper left: cold point temperature; upper right: cold point altitude; lower left: change in cold point temperature with natural log of upwelling; lower right: change in cold point altitude with natural log of upwelling.

of the model results with transport alone show very little change over higher upwelling velocities. This model, in fact, never obtains a cold point temperature that is closer than an order

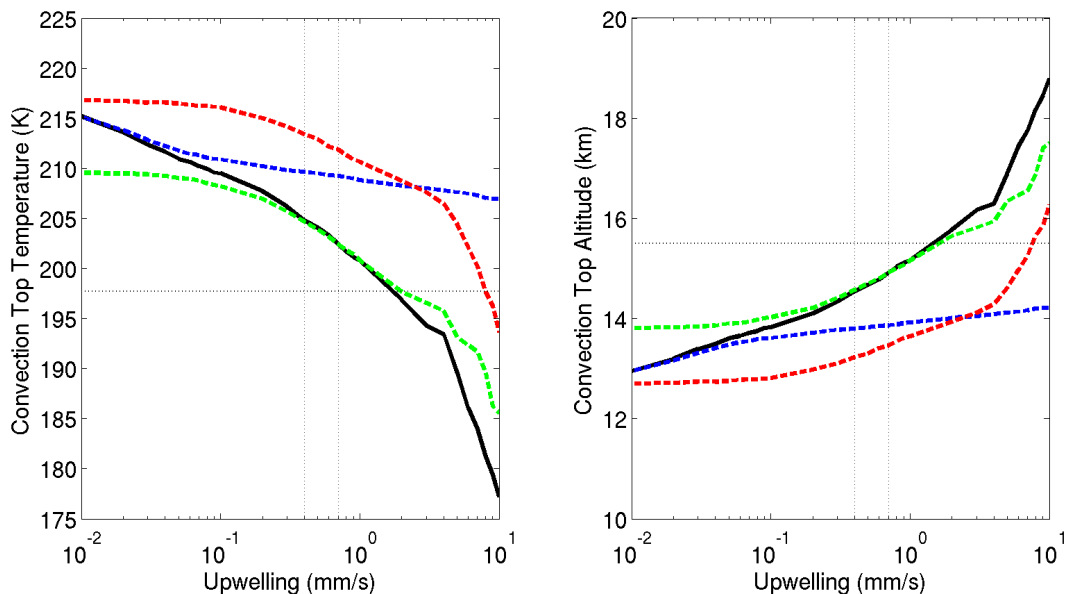


FIGURE 3.12. Convection top quantities versus stratospheric upwelling for RCE profile computed with SHADOZ ozone and dynamics (green dashed), photochemistry with transport and dynamics (solid black), photochemistry with only dynamics (dashed red), and photochemistry with only transport (dashed blue). Left: convection top temperature; right: convection top altitude.

of 10 K to the observed, nor a convection top temperature or altitude equal to the results from the 0.5 mm/s full simulation. However, transport does appear to remove ozone from higher altitudes sufficiently to produce a cold point higher than the observed and a TTL of substantial vertical extent (both at 2 mm/s).

Conversely, the use of dynamics alone can produce a TTL of substantial vertical extent within observed upwelling velocities, and can produce cold point and convection top properties similar to the full simulation quantities at 0.5 mm/s, but only at much faster upwelling velocities. The convection top properties, in particular, require nearly 6 mm/s upwelling to reach the temperature and altitude from the full simulation result with only 0.5 mm/s upwelling. This resistance must be due to the substantially larger ozone concentrations in

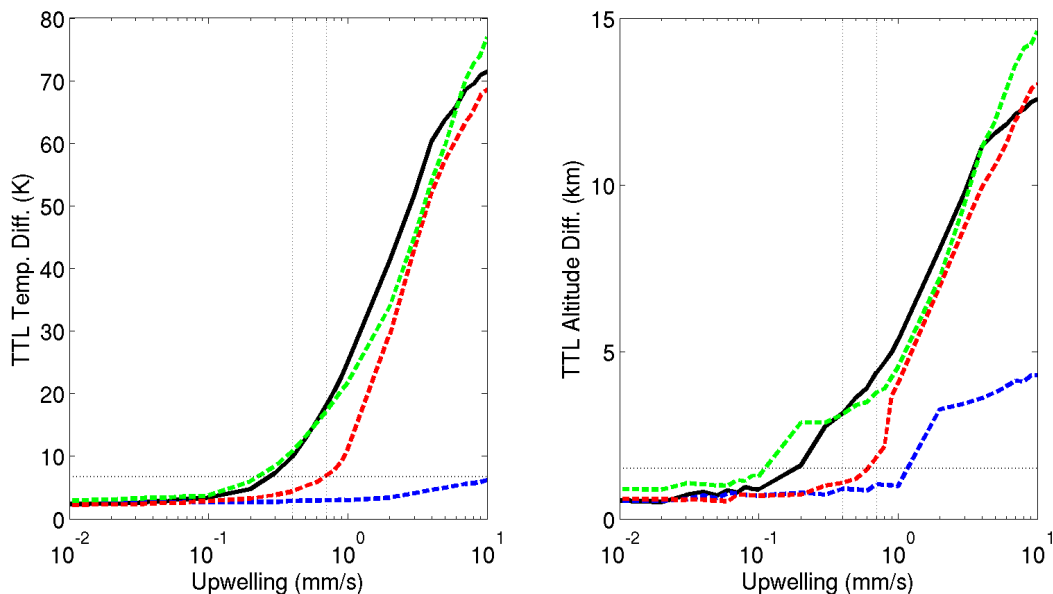


FIGURE 3.13. TTL qualities versus stratospheric upwelling for RCE profile computed with SHADOZ ozone and dynamics (green dashed), photochemistry with transport and dynamics (solid black), photochemistry with only dynamics (dashed red), and photochemistry with only transport (dashed blue). Left: TTL temperature difference (convection top temperature minus cold point temperature); right: TTL vertical width. Horizontal dashed lines show approximate observed values.

the lower stratosphere caused by the absence of transport, supporting the suggestion that transport is a necessary process for simulation of a realistic atmosphere.

Comparing the full simulation and the simulation with observed ozone shows a warmer and lower full simulation cold point and convection top at less than 0.5 mm/s upwelling. Above this, the convection top and cold point are warmer and lower in the observed ozone case, aside from a somewhat higher cold point in the observed ozone case at very fast upwelling velocities. This latter effect is likely due to the altitudes in question, around and above 30 km, being the location of the ozone maximum so that ozone does not increase strongly or decrease with altitude. The former, however, must be due to the effect of ozone transport on the ozone profile. Without ozone transport, the ozone concentrations near the cold point in the observed ozone simulation are higher than they would be at the same

altitudes in the full simulation. By examining the change in cold point temperature with the natural log of upwelling, it appears that this sensitivity is approximately 15% stronger at the observed upwelling when transport is accounted for. Until very fast upwelling velocities this difference only becomes greater. In terms of the cold point altitude sensitivity, the inclusion of upwelling shows approximately a 50% greater sensitivity at the observed upwelling.

However, in regards to the existence of the TTL both the full simulation and the simulation with observed ozone shows that very little upwelling is required to produce a TTL of vertical extent similar to the real atmosphere. The full simulation requires 0.2 mm/s upwelling to produce a such a TTL, while the simulation with observed ozone requires almost achieves this with 0.1 mm/s. However, the observed TTL vertical extent shown is only an approximate value and the model measure used for the bottom of the TTL - the convection top - should only be regarded as an approximate TTL base for the simulated profile. Perhaps a more interesting observation in this regard is that 0.1 mm/s appears to be a critical upwelling velocity because increase in TTL vertical extent with upwelling shows a substantial change at this point. Precisely, below this velocity upwelling increases appear to be unable to widen the TTL substantially whereas above this velocity each increase in upwelling is accompanied by a widening of the TTL. In other words, above 0.1 mm/s each upwelling velocity can produce a different TTL width where as below 0.1 mm/s the TTL width produced by each upwelling velocity is roughly the same.

CHAPTER 4

DISCUSSION

4.1. CONCLUSIONS

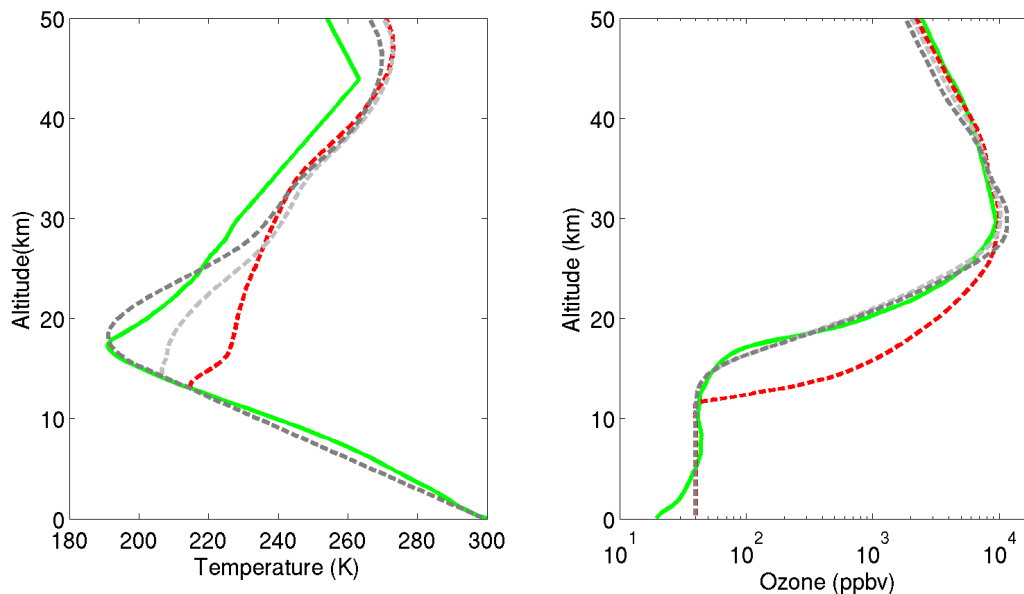


FIGURE 4.1. Profiles for temperature (left) and ozone (right). Profiles shown correspond to observations (solid green), RCE-PCE without dynamics or transport (dashed red), RCE-PCE with transport (dashed light gray), and RCE-PCE with dynamics and transport (dashed dark gray). Dynamics and transport corresponding to 0.5 mm/s upwelling.

The key result of this work is summarized in Figure 4.1. The profiles here show that ozone below 30 km, and particularly in the TTL, reaches equilibrium at much higher concentrations when transport is absent, resulting in a fundamentally different temperature structure compared to observations. In particular, a very low and warm cold point is seen, effectively no TTL exists, and a rapid increase in temperatures is seen in the first 2-3 km above the cold point. When transport is considered, however, the ozone concentration profiles are qualitatively very similar to observations. However, the cold point is still warmer

and lower than observed and a nearly isothermal layer exists for a few kilometers above the cold point. The reduction in TTL ozone also reduces shortwave and longwave heating rates. Because of this, the application of dynamic heating through adiabatic cooling and temperature advection from upwelling is able to reduce temperatures and form a temperature profile that is qualitatively similar to observations.

This result shows that the transport of ozone through the Brewer-Dobson circulation is of first-order importance for the existence of the Tropical Tropopause Layer (TTL). An equally important process is the dynamics from the Brewer-Dobson circulation that cause the temperature structure of the TTL when combined with the effect of ozone transport. This work therefore suggests that the TTL exists due to the Brewer-Dobson circulation. The work also suggests that relatively few processes are required to capture the temperature structure of the tropical atmosphere given the simplicity of this model.

Due to the strengthening of the Brewer-Dobson circulation caused by climate change, this work also suggests that the cold point tropopause will cool and loft in the future, as is generally expected. However, this work also suggests that the transport of ozone through the Brewer-Dobson circulation contributes substantially to this effect, perhaps as much as 30%, depending on the magnitude in the increase of upwelling. This shows that attempts to calculate the change in TTL cold point temperatures will be underestimates if interactive ozone is not applied.

Other suggestions from this work include that a very low upwelling velocity, perhaps less than 0.1 mm/s, is sufficient to remove most ozone from the observed TTL. Similarly, 0.10 mm/s appears to be a sufficient velocity for the existence of a TTL or at least the beginning of TTL-like behavior. Another, more puzzling suggestion is that the altitude at

which transport ceases to be a critical process for the determination of ozone concentrations is rather directly dependent on upwelling velocity. This result, however, relies the most strongly on the simplified chemistry of this model out of all other results in this work, and so should not be considered fact without further investigation.

4.2. FUTURE WORK

There are two main avenues of research that follow from this model. The first is to utilize this model to investigate other sensitivities. Chief among these are the sensitivities of the TTL to other climate change processes. The sensitivity to carbon dioxide concentrations, in particular, would be interesting, as would the sensitivity to surface temperatures. In consideration of surface temperatures, another sensitivity that may merit investigation is the surface temperature sensitivity to stratospheric upwelling due to transport of ozone in the TTL and stratosphere. This would require a more complex simulation of convection but could be achieved in the same single-column framework. Sensitivities could also be explored with simultaneous calculations of interactive water and ozone. This would be very easy to implement and could show a feedback between radiation and stratospheric water vapor, with additional implications for climate change.

The second avenue is the characterization of atmospheric processes using more complex methods to determine if the results are maintained under more realistic conditions. In particular, the ozone destruction chemistry involved in this work is rather simplified, in particular with regards to the destruction of ozone. These rates were compared to those from WACCM, a global climate-chemistry model with considerably more complicated ozone chemistry, and the WACCM destruction rates were shown to be stronger than those computed in this work, particularly below 15 km (Doug Kinnison, personal correspondence). Chemical destruction

is not the first-order removal process of ozone in the TTL, however, so weak destruction likely do not present a large source of error in the simulations that involve ozone transport. But in absence of transport chemical destruction is the only process of ozone removal in the entire atmosphere and so an underestimate in these destruction rates may result in larger ozone concentrations for pure photochemical equilibrium experiments.

Two more directions for model improvement could be found in characterizations of the horizontal transport of ozone and the impact of convection on ozone concentrations. The former could be difficult to implement in this model because of the dependence of horizontal mixing on the Brewer-Dobson circulation, so that parameterization may be difficult. The simulation of ozone content changes through convection, meanwhile, was attempted in this work. However, numerical problems were found to be associated with the simplified method used, where all ozone mixing ratios at and below the convection top were fixed to the tropospheric minimum ozone mixing ratio. It is possible, then, that a more realistic simulation of convection would be required to capture this relationship, perhaps through a three-dimensional convection model. Another possible model improvement regarding convection is the alteration of convective adjustment to use a moist, vertically-varying adiabatic instead of a vertically-constant, prescribed value. This would produce a more realistic method of convective adjustment but would add complexity to the model.

It is known that clouds are often present in the observed TTL, although the extent of some kinds of clouds in the region are not completely clear [8]. The effects of these clouds on radiation and temperatures in the region are not precisely understood from a quantitative respect, either, and to the knowledge of the author these effects have not been

investigated in an RCE framework. This model in particular only investigates the clear-sky radiation balance, although it may be possible to investigate the effects of clouds in a rough, qualitative way with relatively small additions to the model. This represents a major unanswered question in the heating rate balance of the TTL.

A final but secondary direction for future work is the investigation of the reason for the logarithmic relationship between the transition altitude and upwelling velocity, shown in Figure 3.10. Because this relationship is so clear, it seems likely that an approximation of the ozone continuity equation could suggest a reason for this. However, such an analytical relationship remains elusive.

BIBLIOGRAPHY

- [1] Atkinson, R., and Coauthors, 2004: Iupac task group on atmospheric chemical kinetic data evaluation. URL <http://iupac.pole-ether.fr/>, 1461-1738 pp.
- [2] Birner, T., 2010: Residual circulation and tropopause structure. *Journal of the Atmospheric Sciences*, **67** (8), 2582–2600, doi: 10.1175/2010JAS3287.1, URL <http://dx.doi.org/10.1175/2010JAS3287.1>, <http://dx.doi.org/10.1175/2010JAS3287.1>.
- [3] Birner, T., and E. Charlesworth, submitted to J. Geophys. Res., December 2016: On the importance of water vapor and ozone radiative heating for tropical tropopause temperatures.
- [4] Brasseur, G. P., and S. Solomon, Eds., 2005: *Aeronomy of the Middle Atmosphere*. Springer, 636 pp.
- [5] Brewer, A. W., 1949: Evidence for a world circulation provided by the measurements of helium and water vapour distribution in the stratosphere. *Quarterly Journal of the Royal Meteorological Society*, **75** (326), 351–363, doi:10.1002/qj.49707532603, URL <http://dx.doi.org/10.1002/qj.49707532603>.
- [6] Burkholder, J. B., and Coauthors, 2015: "Chemical Kinetics and Photochemical Data for Use in Atmospheric Studies, Evaluation No. 18," JPL Publication 15-10, Jet Propulsion Laboratory, Pasadena, 2015 <http://jpldataeval.jpl.nasa.gov>.
- [7] Eyring, V., T. G. Shepherd, and D. W. Waugh, : SPARC CCMVal Report on the Evaluation of Chemistry-Climate Models. Tech. rep., SPARC, 426 pp.
- [8] Fueglistaler, S., A. E. Dessler, T. J. Dunkerton, I. Folkins, Q. Fu, and P. W. Mote, 2009: Tropical tropopause layer. *Reviews of Geophysics*, **47** (1), doi:10.1029/2008RG000267.

- [9] Gettelman, A., and Coauthors, 2010: Multimodel assessment of the upper troposphere and lower stratosphere: Tropics and global trends. *Journal of Geophysical Research: Atmospheres*, **115 (D3)**, n/a–n/a, doi:10.1029/2009JD013638, d00M08.
- [10] Jacobs, D. J., Ed., 1999: *Introduction to Atmospheric Chemistry*. Princeton University Press, 266 pp.
- [11] Konopka, P., and Coauthors, 2007: Contribution of mixing to upward transport across the tropical tropopause layer (ttl). *Atmospheric Chemistry and Physics*, **7 (12)**, 3285–3308.
- [12] Manabe, S., and R. F. Strickler, 1964: Thermal equilibrium of the atmosphere with a convective adjustment. *Journal of the Atmospheric Sciences*, **21 (4)**, 361–385.
- [13] McElroy, M. B., R. J. Salawitch, and K. Minschwaner, 1992: The changing stratosphere. *Planetary and space science*, **40 (2-3)**, 373–401.
- [14] Minschwaner, K., R. Salawitch, and M. McElroy, 1993: Absorption of solar radiation by o₂: Implications for o₃ and lifetimes of n₂o, cfcl₃, and cf₂cl₂. *Journal of Geophysical Research: Atmospheres*, **98 (D6)**, 10 543–10 561.
- [15] Mlawer, E. J., S. J. Taubman, P. D. Brown, M. J. Iacono, and S. A. Clough, 1997: Radiative transfer for inhomogeneous atmospheres: Rrtm, a validated correlated-k model for the longwave. *Journal of Geophysical Research: Atmospheres*, **102 (D14)**, 16 663–16 682.
- [16] Solomon, S., R. Garcia, and F. Stordal, 1985: Transport processes and ozone perturbations. *Journal of Geophysical Research: Atmospheres*, **90 (D7)**, 12 981–12 989.

- [17] Thuburn, J., and G. C. Craig, 2002: On the temperature structure of the tropical stratosphere. *Journal of Geophysical Research: Atmospheres*, **107** (D2), ACL 10–1–ACL 10–10, doi:10.1029/2001JD000448, URL <http://dx.doi.org/10.1029/2001JD000448>.
- [18] Watson, R., and Coauthors, 1986: WMO Atmospheric Ozone: 1985; National Aeronautics and Space Administration: Geneva, Report No. 16.
- [19] Yoshino, K., and Coauthors, 1988: Improved absorption cross-sections of oxygen in the wavelength region 205–240 nm of the Herzberg continuum. *Planetary and Space Science*, **36** (12), 1469–1475.